Odd elasticity and topological waves in active surfaces

Michele Fossati,[1,2] Colin Scheibner,[3,4] Michel Fruchart,[3,4] and Vincenzo Vitelli[3,4,5,6,*]

[1]*SISSA, Trieste 34136, Italy*
[2]*INFN Sezione di Trieste, Trieste 34127, Italy*
[3]*James Franck Institute, University of Chicago, Chicago, Illinois 60637, USA*
[4]*Department of Physics, University of Chicago, Chicago, Illinois 60637, USA*
[5]*Kadanoff Center for Theoretical Physics, University of Chicago, Chicago, Illinois 60637, USA*
[6]*Institute for Biophysical Dynamics, University of Chicago, Chicago, Illinois 60637, USA*

(Received 11 July 2023; accepted 12 January 2024; published 28 February 2024)

Odd elasticity describes active elastic systems whose stress-strain relationship is not compatible with a potential energy. As the requirement of energy conservation is lifted from linear elasticity, new antisymmetric (odd) components appear in the elastic tensor. In this work we study the odd elasticity and non-Hermitian wave dynamics of active surfaces, specifically plates of moderate thickness. These odd moduli can endow the vibrational modes of the plate with a nonzero topological invariant known as the first Chern number. Within continuum elastic theory, we show that the Chern number is related to the presence of unidirectional shearing waves that are hosted at the plate's boundary. We show that the existence of these chiral edge waves hinges on a distinctive two-step mechanism. Unlike electronic Chern insulators where the magnetic field at the same time gaps the spectrum and imparts chirality, here the finite thickness of the sample gaps the shear modes, and the odd elasticity makes them chiral.

DOI: 10.1103/PhysRevE.109.024608

I. INTRODUCTION

Membranes driven by active, energy consuming, processes play a role in processes ranging from cell division and deformation [1–5] to morphogenesis [6–8] and soft robotics [9–11]. In order to model these systems, one typically combines the elasticity of passive surfaces [12–17] with active forces, leading to self-organized behaviors ranging from shape instabilities to traveling waves and oscillations [18–24]. Yet elasticity itself can also be modified by internal energy sources: the elastic tensor relating stress and strain can include so-called odd elastic coefficients, which describe the part of the elastic response that is not compatible with energy conservation [19,25–27]. Odd elasticity is expected to naturally emerge in effective descriptions of active mechanical systems. While odd elasticity has not yet been observed in naturally occurring biological membranes, signatures of odd elasticity have been reported in bulk systems such as robotic metamaterials [28,29], collections of spinning magnetic colloids [30], starfish embryos [31], and models of muscular hydraulics [32].

In this article we investigate the odd elasticity of membranes and its effect on vibrational dynamics. The potential role of odd elastic moduli in membranes has been proposed on the grounds of symmetry in sheets of vanishing thickness [19]. In the limit of vanishing thickness, the cross section of the membrane is slaved to the out-of-plane bending of the membrane. For linear deformations, the relevant odd moduli do not affect the out-of-plane motion of the membrane subject to the vanishing thickness assumption. Here we extend the analysis to plates with finite thickness, focusing on the so-called moderately thick regime, in which the tilting of the plate cross section is independent from its midplane deformation. A symmetry analysis reveals that an isotropic, free-standing, moderately thick plate can exhibit two independent odd elastic moduli that affect the linearized, out-of-plane dynamics of the membrane, one of which disappears in the limit of vanishing thickness. By analyzing the normal modes of vibration of odd-elastic plates, we show that odd elasticity affects both wave propagation in the plate and its linear stability. Furthermore, we show that odd elastic plates can support edge modes in which waves propagate in a unidirectional fashion at the border of the plate. The waves propagating in these edge modes do not backscatter when they encounter sharp edges or defects, owing to the topological nature of the edge modes [33–46]. We show that the existence of these chiral edge waves hinges on a distinctive two-step mechanism. Unlike electronic Chern insulators where the magnetic field at the same time gaps the spectrum and imparts chirality, here the finite thickness of the sample gaps the shear modes, and the odd elasticity makes them chiral.

II. ODD ELASTICITY OF MODERATELY THICK PLATES

In this section we set up the description of an odd elastic plate. We first review the framework of odd elasticity [25,26] (Sec. II A) and the Reissner-Mindlin theory of moderately thick plates [12,47,48] (Sec. II B). We then derive the elastic constitutive relations of the plate, starting from

*vitelli@uchicago.edu

the three-dimensional (3D) bulk elastic tensor of the material constituting the plate (Sec. II C). Finally, we obtain the equations of motion describing the dynamics of the deformation of the plate (Sec. II D).

A. Odd elasticity

Linear elasticity is the continuum theory that describes the behavior of solids under small long-wavelength deformations. The deformation of the solid is described by the displacement field $\xi_i(\mathbf{x}) = x_i' - x_i$ giving the difference between the original position of a point $\mathbf{x}$ of the elastic solid and its current position $\mathbf{x}'$. We assume that only the variation of the internal relative distances modifies the physical state. The internal forces then depend only on the strain tensor $u_{ij} = (\partial_i \xi_j + \partial_j \xi_i)/2$ at linear order. The forces between parcels of the elastic continuum are described by the stress tensor σ_{ij}. In linear elasticity, one assumes a linear relation between stress and strain

$$\sigma_{ij} = C_{ijk\ell} u_{k\ell}, \tag{1}$$

where $C_{ijk\ell}$ is the elastic tensor, assumed here to be homogeneous in space and frequency independent. Symmetry constrains the structure of $C_{ijk\ell}$. The strain tensor is symmetric by construction, and, if internal torques are absent, the stress tensor is symmetric too. In this case, the elastic tensor is symmetric under the exchanges $i \leftrightarrow j$ and $k \leftrightarrow \ell$ [49]. See Refs. [19,25] for cases in which the displacement gradient tensor and the stress tensor are not assumed to be symmetric.

If the system is conservative, another symmetry exists: the elastic tensor satisfies $C_{ijk\ell} = C_{k\ell ij}$. To see why, note that the forces are conservative if the net work done is zero for every sequence of deformation that begins and ends in the same configuration. The work per unit volume of an infinitesimal deformation is given by $\sigma_{ij} du_{ij}$ and the work per unit volume under a finite cycle of deformation is calculated as the line integral of this quantity. We consider a closed path $\mathscr{C}$ in the strain space, parameterized by $u_{ij}(\lambda)$. Let $\sigma_{ij}(\lambda) = C_{ijk\ell} u_{k\ell}(\lambda)$ be the associated stress tensor. By applying Stokes's theorem, we can express the work $\mathscr{W}$ as the surface integral

$$\mathscr{W} = \oint_{\mathscr{C}} \sigma_{ij}\, du_{ij} = \int_{\mathscr{S}} \frac{1}{2} \frac{\partial \sigma_{ij}}{\partial u_{k\ell}}\, du_{ij} \wedge du_{k\ell} \tag{2}$$

in which $\wedge$ is the exterior product and $\mathscr{S}$ is a surface in strain space such that $\partial \mathscr{S} = \mathscr{C}$. Using the antisymmetry of the exterior product, we can see that the forces are conservative ($\mathscr{W} = 0$ for all $\mathscr{C}$) if and only if

$$\frac{\partial \sigma_{ij}}{\partial u_{k\ell}} = \frac{\partial \sigma_{k\ell}}{\partial u_{ij}}, \tag{3}$$

or equivalently, if and only if

$$C_{ijk\ell} = C_{k\ell ij}. \tag{4}$$

This property is known as Maxwell-Betti reciprocity [50]. A system is said to be *odd elastic* when Eq. (4) does not hold, i.e., when its elastic tensor has components that are odd under exchange $ij \leftrightarrow k\ell$ [25]. Note that we have made no distinction between the Cauchy and Piola-Kirchhoff stress tensors, because we have assumed that there is no prestress in the system; see Refs. [26,51] for details.

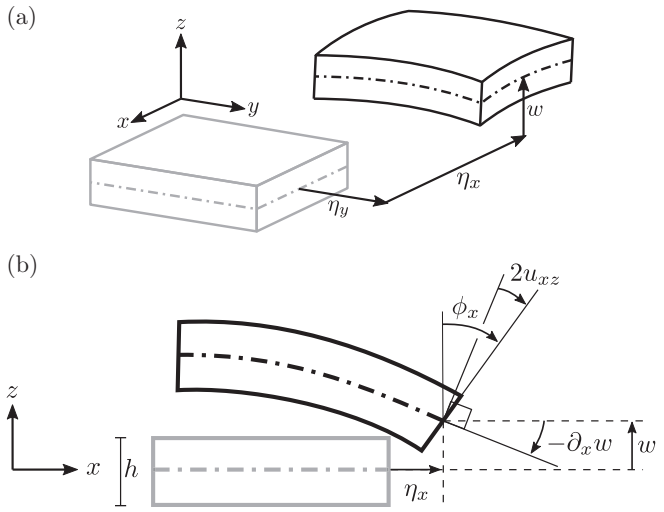

FIG. 1. Kinematics of a moderately thick plate. In the Reissner-Mindlin theory of moderately thick plates, the deformation of a plate (drawn in its undeformed reference state in gray and in a deformed state in black) is parameterized by five fields (η_x, η_y, ϕ_x, ϕ_y, and w) defined on the midplane (dash-dotted line). The fields $\eta_x(\eta_y)$ and w describe, respectively, the horizontal and vertical displacements of the midplane (a). The field ϕ_x is the angle between a deformed normal line in the x direction and the z axis. The quantity $-\partial_x w$ quantifies the slope of the midplane in the x direction. If $-\partial_x w$ is different from ϕ_x, then u_{xz} is nonzero (b).

B. Reissner-Mindlin theory

We consider a moderately thick and initially flat surface, i.e., a plate, whose midplane (the longitudinal plane that cuts the plate's thickness in half) lies at rest in the x-y plane; see Fig. 1. The plate has uniform thickness h along the z axis at rest. In the Reissner-Mindlin theory of moderately thick plates [12], the full 3D displacement field of the plate $\xi_i(x, y, z)$ is expressed in terms of fields defined on the horizontal midplane as

$$\begin{aligned} \xi_x(x, y, z) &= \eta_x(x, y) + z\phi_x(x, y), \\ \xi_y(x, y, z) &= \eta_y(x, y) + z\phi_y(x, y), \\ \xi_z(x, y, z) &= w(x, y). \end{aligned} \tag{5}$$

The field η_α represents the horizontal displacement of the midplane ($z = 0$) in the direction $\alpha \in \{x, y\}$, while w describes the vertical displacement. A line of points that lies vertical at rest is inclined of an angle ϕ_α between the z axis and the α axis after the deformation (Fig. 1). While the full displacement field is defined over a 3D space, the fields η_α, ϕ_α, and w are defined over the midplane, which is a two-dimensional (2D) manifold.

The strains can be decomposed into two terms: z-independent and z-linear $u_{ij} = u^0_{ij} + z u^1_{ij}$. Here u^1_{ij} describes strains in which the top face and the bottom face of the plate are deformed oppositely. Explicitly

$$\begin{aligned} 2u^0_{\alpha\beta} &= \partial_\alpha \eta_\beta + \partial_\beta \eta_\alpha, \\ 2u^0_{\alpha z} &= \phi_\alpha + \partial_\alpha w, \\ u^0_{zz} &= 0, \end{aligned}$$

$$2u^1_{\alpha\beta} = \partial_\alpha\phi_\beta + \partial_\beta\phi_\alpha,$$
$$u^1_{\alpha z} = 0,$$
$$u^1_{zz} = 0. \tag{6}$$

The bending of the midplane is quantified by $-\partial_\alpha w$, and $u^0_{\alpha z}$ is half of the angle between a deformed vertical line and the normal to the deformed midplane, projected in the α direction (Fig. 1). No z-linear term is present in the transverse strain. The vertical strain u_{zz} is identically zero because the vertical displacement is independent from z (a strain tensor with $u_{zz} = 0$ is known as a *plane strain*). Since $\xi_\alpha = \eta_\alpha + z\phi_\alpha$, an originally vertical straight line remains straight after the deformation, and since $u_{zz} = 0$, the line does not elongate.

C. Constitutive relations of odd elastic plates

We now derive an elastic constitutive relation for the plate, starting from the 3D bulk elastic tensor of the material constituting the plate.

1. Basis tensors and bulk constitutive relations

We first define a basis of symmetric rank-two tensors appropriate to the plate geometry, that we will then use to represent the tensorial constitutive relations in matrix form:

$$Z = \begin{pmatrix} 0 & 0 & 0 \\ 0 & 0 & 0 \\ 0 & 0 & 1 \end{pmatrix}, \qquad D = \frac{1}{\sqrt{2}}\begin{pmatrix} 1 & 0 & 0 \\ 0 & 1 & 0 \\ 0 & 0 & 0 \end{pmatrix},$$
$$S^1 = \frac{1}{\sqrt{2}}\begin{pmatrix} 1 & 0 & 0 \\ 0 & -1 & 0 \\ 0 & 0 & 0 \end{pmatrix}, \qquad S^2 = \frac{1}{\sqrt{2}}\begin{pmatrix} 0 & 1 & 0 \\ 1 & 0 & 0 \\ 0 & 0 & 0 \end{pmatrix},$$
$$T^x = \frac{1}{\sqrt{2}}\begin{pmatrix} 0 & 0 & 1 \\ 0 & 0 & 0 \\ 1 & 0 & 0 \end{pmatrix}, \qquad T^y = \frac{1}{\sqrt{2}}\begin{pmatrix} 0 & 0 & 0 \\ 0 & 0 & 1 \\ 0 & 1 & 0 \end{pmatrix}. \tag{7}$$

These basis tensors are collectively referred to as B^a with $a = 0, \ldots, 5$ (so $B^0 = Z$, $B^1 = D$, $B^2 = S^1$, etc.). We then decompose the strain and stress tensors on this basis as

$$\sigma_{ij} = \sigma_a B^a_{ij} \qquad \text{and} \qquad u_{ij} = u_a B^a_{ij} \tag{8}$$

in which the sum over a is implied. The tensor D describes cylindrical symmetric strains and stresses, $S^{1,2}$ the planar shears, and $T^{x,y}$ the cross-sectional shears in x and y direction. This basis separates the irreducible representations of the group of rotations SO(2) around the z axis: D is invariant, S^α transforms as a two-headed arrow in the plane, and T^α transforms as an ordinary vector in the plane. All basis tensors except Z have a vanishing zz entry and therefore represent plane stresses and strains, while Z describes nonplane stresses and strains.

The constitutive relation (1) for the 3D bulk can then be written in matrix form as

$$\sigma^{3D}_a = C^{3D}_{ab} u^{3D}_b \tag{9}$$

in which σ^{3D}_a and u^{3D}_b are the components of the stress and strain in the basis (7), with $a, b = 0, \ldots, 5$.

2. Effective in-plane constitutive relation

The elastic tensor of the plate is then derived from the elastic tensor of the bulk 3D material by eliminating the variables $\sigma_0 \equiv \sigma_{zz}$ and $u_0 \equiv u_{zz}$ under the so-called plane-stress hypothesis $\sigma_{zz} = 0$ [52]. This is detailed in Appendix B. The constitutive relation for the plate then reads

$$\sigma_a = C_{ab} u_b \tag{10}$$

in which we now have only $a, b = 1, \ldots, 5$ (as the nonplane components σ_0 and u_0 have been eliminated), and in which C_{ab} is an effective elastic tensor related to C^{3D}_{ab} by the nonlinear relation (B2) in Appendix B.

Assuming that the 3D bulk is described by the most general elastic tensor C^{3D}_{ab} compatible with cylindrical isotropy (i.e., invariant under rotations around the z axis), which is given in Appendix A, we show in Appendix B that the elastic matrix of the plate in Eq. (10) reads

$$C_{ab} = 2\begin{pmatrix} \tilde{B} & 0 & 0 & 0 & 0 \\ 0 & \mu_1 & K^o_1 & 0 & 0 \\ 0 & -K^o_1 & \mu_1 & 0 & 0 \\ 0 & 0 & 0 & \mu_2 & K^o_2 \\ 0 & 0 & 0 & -K^o_2 & \mu_2 \end{pmatrix} \tag{11}$$

in the basis $\{D, S^1, S^2, T^x, T^y\}$. Here $\tilde{B}$ is an effective 2D bulk modulus [given by Eq. (B4)] which relates 2D isotropic dilations to the 2D isotropic stress, μ_1 and μ_2 are passive shear moduli that couple respectively planar shears (u_{S^1}, u_{S^2}) and cross-sectional shears (u_{T^x}, u_{T^y}), while the odd moduli K^o_1, K^o_2 build the antisymmetric part of the elastic tensor; namely, K^o_1 maps u_{S^1} to $-\sigma_{S^2}$ and u_{S^2} to σ_{S^1}. K^o_2 acts analogously on the basis elements T^x, T^y.

3. Constitutive relation for the net stress and moment

The dynamical quantities that are relevant for the plate's dynamics are the *net stress tensor* N_{ij} and the *moment tensor* M_{ij} defined by

$$N_{ij} = \int_{-h/2}^{h/2} dz\, \sigma_{ij}, \quad M_{ij} = \int_{-h/2}^{h/2} dz\, z\sigma_{ij}. \tag{12}$$

These are respectively the zeroth and first moment of the stress in z. Integration in the z direction produces a net stress that depends only on u^0 and a moment tensor that depends on the bending terms u^1. Using the constitutive equations (1) with the elastic tensor in Eq. (11), we find that the in-plane stresses are governed by

$$\begin{pmatrix} N_D \\ N_{S^1} \\ N_{S^2} \end{pmatrix} = 2h\begin{pmatrix} \tilde{B} & 0 & 0 \\ 0 & \mu_1 & K^o_1 \\ 0 & -K^o_1 & \mu_1 \end{pmatrix}\begin{pmatrix} u^0_D \\ u^0_{S^1} \\ u^0_{S^2} \end{pmatrix}, \tag{13}$$

TABLE I. Plate strains and stresses. Here u^0 and u^1 are respectively the zeroth- and first-order contributions to the strain in a power expansion in z; N is the net stress and M is the bending moment. The column is labeled by the tensor basis element on which the stresses, strains, and moments are projected. The arrows are visual cues for the forces and torques on each of the shown surfaces (light arrows are pointing towards the inside of the plate).

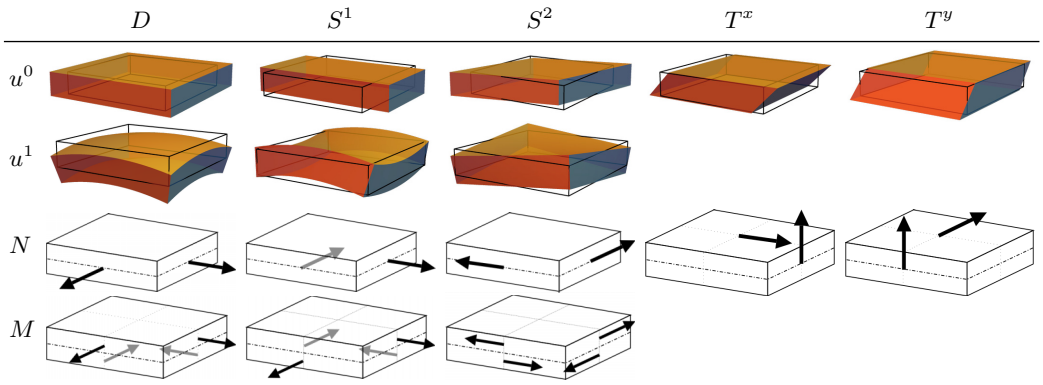

while the bending moments are governed by

$$\begin{pmatrix} M_D \\ M_{S^1} \\ M_{S^2} \end{pmatrix} = \frac{h^3}{6} \begin{pmatrix} \tilde{B} & 0 & 0 \\ 0 & \mu_1 & K_1^o \\ 0 & -K_1^o & \mu_1 \end{pmatrix} \begin{pmatrix} u_D^1 \\ u_{S^1}^1 \\ u_{S^2}^1 \end{pmatrix} \tag{14}$$

and the cross-sectional stresses by

$$\begin{pmatrix} N_{T^x} \\ N_{T^y} \end{pmatrix} = 2h \begin{pmatrix} \mu_2 & K_2^o \\ -K_2^o & \mu_2 \end{pmatrix} \begin{pmatrix} u_{T^x}^0 \\ u_{T^y}^0 \end{pmatrix}. \tag{15}$$

A visual representation of the components of the strain, net stress, and moment tensor in the basis of Eq. (7) is given in Table I. We note that the constitutive equations in Eqs. (13) to (15) assume that the plate arises as the thin limit of a homogeneous 3D solid. However, if the plate is not homogeneous along its thickness, additional moduli can appear that couple the independent equations in Eqs. (13) to (15); see Appendix B. Notice that the moduli μ_2 and K_2^o set the stresses in response to the cross-sectional shearing. The matrix in Eq. (15) is proportional to a rotation matrix whose chirality is set by the modulus K_2^o. This will play a crucial role when we discuss the spectrum and topological modes in Sec. III. In the limit of zero thickness, the constitutive relations Eqs. (13) to (15) match the flat limit of the constitutive relations in Ref. [19] (see Appendix C).

Having the constitutive relations, we can examine the linearly independent cycles in strain space over which work is extracted $\mathscr{C} = \partial\mathscr{S}$. The work per unit surface is

$$\begin{aligned} \mathcal{W} &= \int_{-h/2}^{h/2} dz \int_{\mathscr{C}} du_a\, C_{ab} u_b \\ &= h \int_{\mathscr{C}} du_a^0\, C_{ab} u_b^0 + \frac{h^3}{12} \int_{\mathscr{C}} du_a^1\, C_{ab} u_b^1 \\ &= \frac{h}{2} \int_{\mathscr{S}} C_{ab}\, du_a^0 \wedge du_b^0 + \frac{h^3}{24} \int_{\mathscr{S}} C_{ab}\, du_a^1 \wedge du_b^1. \end{aligned} \tag{16}$$

There are three independent ways to extract energy with a cycle of deformations, represented in Fig. 2. Cycling in the plane $u_{S^1}^0$-$u_{S^2}^0$, the energy density extracted is equal to $2hK_1^o$ times the area enclosed in the strain space [Fig. 2(a)]. A bending cycle that involves $u_{S^1}^1$ and $u_{S^2}^1$ extracts $(h^3/6)K_1^o$ times the area enclosed [Fig. 2(b)]. With a cycle in the $u_{T^x}^0$-$u_{T^y}^0$ plane, the density of work is $2hK_2^o$ times the area enclosed [Fig. 2(c)].

D. Equations of motion

We now study the dynamics of the system. To do so, let us assume that the elastic material evolves according to a Newtonian dynamics and is subject to an external friction force $f_i^{\text{ext}} = -\Gamma\dot{\xi}_i$ summarizing the effect of the environment. The evolution of the plates is then described by the following

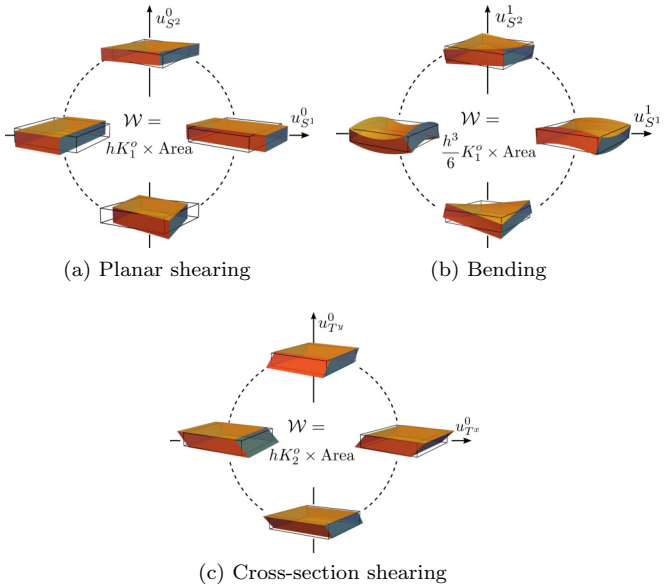

(a) Planar shearing (b) Bending

(c) Cross-section shearing

FIG. 2. Energy cycles in the elastic plate. Illustrations of the three linearly independent cycles that extract energy from the plate. Panel (a) utilizes in planar shear deformations, panel (b) utilizes bending deformations, and panel (c) utilizes cross-sectional shearing. See Table I for definitions of the deformation icons.

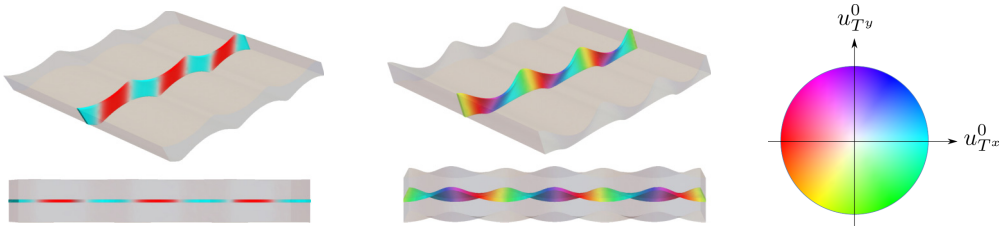

(a) Passive eigenmode (b) Active eigenmode (c) Legend: strain space

FIG. 3. Perspective and top view of bulk, gapped eigenmodes. We illustrate the eigenmodes implied by Eq. (25). As a guide, a deformed cross-sectional slice of the plate is colored by the local component of cross-sectional shears $u^0_{Tx,y}$ (see Fig. 2 and Table I for illustration of cross-sectional shears). (a) A passive eigenmode ($K^o_1 = K^o_2 = 0$) traces out a line (red-blue) in strain space. (b) An eigenmode with $K^o_2 > 0$ and $\tilde{B} = \mu = K^o_1 = 0$ draws an ellipse in the strain plane (full color wheel present). The energy injected in the system after a complete oscillation is proportional to the area covered in the strain plane.

conservation laws for linear and angular momentum (derived in Appendix D)

$$h(\rho\ddot{\eta}_\alpha + \Gamma\dot{\eta}_\alpha) = \partial_\beta N_{\beta\alpha}, \tag{17}$$

$$h(\rho\ddot{w} + \Gamma\dot{w}) = \partial_\alpha N_{\alpha z}, \tag{18}$$

$$\frac{h^3}{12}(\rho\ddot{\phi}_\alpha + \Gamma\dot{\phi}_\alpha) = \partial_\beta M_{\beta\alpha} - N_{z\alpha}, \tag{19}$$

where ρ is the density of the plate, assumed to be uniform.

Using the constitutive relations, Eqs. (13) to (15), we obtain

$$\rho\ddot{\eta}_\alpha + \Gamma\dot{\eta}_\alpha = \big(B\partial_\alpha\partial_\beta + \mu_1\nabla^2\delta_{\alpha\beta} + K^o_1\nabla^2\epsilon_{\alpha\beta}\big)\eta_\beta, \tag{20}$$

$$\rho\ddot{w} + \Gamma\dot{w} = \mu_2\nabla^2 w + \mu_2\partial_\alpha\phi_\alpha + K^o_2\epsilon_{\alpha\beta}\partial_\alpha\phi_\beta, \tag{21}$$

$$\frac{h^2}{12}(\rho\ddot{\phi}_\alpha + \Gamma\dot{\phi}_\alpha) = \frac{h^2}{12}\big(B\partial_\alpha\partial_\beta + \mu_1\nabla^2\delta_{\alpha\beta} + K^o_1\nabla^2\epsilon_{\alpha\beta}\big)\phi_\beta - \big(\mu_2\delta_{\alpha\beta} + K^o_2\epsilon_{\alpha\beta}\big)(\partial_\beta w + \phi_\beta). \tag{22}$$

We first note that horizontal displacements η_α are decoupled from the other degrees of freedom. Their dynamics are identical to that of a purely 2D isotropic odd elastic system, which has already been studied in [25]. The out-of-plane dynamics governed by Eqs. (21) and (22) will be the focus of the following sections.

In the limit $h \to 0$ of thin plates, Eq. (22) implies $\partial_\alpha w + \phi_\alpha = 0$ and the equations of motion become those of the Kirchhoff-Love theory of plates [12] where $u_{\alpha z}$ is identically zero. Namely, the out-of-plane deflection ω obeys the equation

$$\rho\ddot{w} + \Gamma\dot{w} = -D_{\text{eff}}\nabla^4 w, \tag{23}$$

where

$$D_{\text{eff}} = h^2\frac{(B+\mu_1)\big[\mu_2^2 - \big(K^o_2\big)^2\big] - 2\mu_2 K^o_1 K^o_2}{12\big[\mu_2^2 + \big(K^o_2\big)^2\big]} \tag{24}$$

as derived in Appendix D. Notice that this equation is structurally identical to that of a passive plate, but with the effective bending stiffness D_{eff} renormalized by odd moduli K^o_1 and K^o_2.

III. NORMAL MODES AND TOPOLOGICAL WAVES

We now analyze the normal modes of vibration of the odd elastic plate. As illustrated in Fig. 3, we first show how the flexural eigenmodes behave in the bulk of the plate (i.e., far from any edge). Then, we show how to assign a topological invariant to the band structure of the system. This step allows us to predict the existence of unidirectional edge states exponentially localized to the boundary of the plate (Fig. 7), under certain boundary conditions [53–56].

A. Normal modes of vibration

The out-of-plane deformations of the plate are described by Eqs. (21) and (22). As these equations are linear, all solutions are obtained by considering solutions of the form $\phi_\alpha(\mathbf{x}, t) = \phi_\alpha\, e^{i(\mathbf{k}\cdot\mathbf{x} - \underline{\omega}t)}$ and $w(\mathbf{x}, t) = w\, e^{i(\mathbf{k}\cdot\mathbf{x} - \underline{\omega}t)}$ and solving the resulting eigenvalue problem. Using the dimensionless quantities $\mathbf{q} = (\sqrt{12}h)\mathbf{k}$ and $\tilde{w} = w/(\sqrt{12}h)$, we obtain

$$\frac{h^2}{12}(\rho\underline{\omega}^2 + i\Gamma\underline{\omega})\begin{pmatrix}\boldsymbol{\phi}\\ \tilde{w}\end{pmatrix} = \mathcal{M}(\mathbf{q})\begin{pmatrix}\boldsymbol{\phi}\\ \tilde{w}\end{pmatrix} \tag{25}$$

in which we have introduced the dynamical matrix

$$\mathcal{M}(\mathbf{q}) = \mathcal{M}^e(\mathbf{q}) + \mathcal{M}^o(\mathbf{q}) \tag{26}$$

in which

$$\mathcal{M}^e(\mathbf{q}) = \begin{pmatrix}\tilde{B}q_x^2 + \mu_1 q^2 + \mu_2 & \tilde{B}q_x q_y & i\mu_2 q_x\\ \tilde{B}q_x q_y & \tilde{B}q_y^2 + \mu_1 q^2 + \mu_2 & i\mu_2 q_y\\ -i\mu_2 q_x & -i\mu_2 q_y & \mu_2 q^2\end{pmatrix}$$

and

$$\mathcal{M}^o(\mathbf{q}) = \begin{pmatrix}0 & K^o_1 q^2 + K^o_2 & iK^o_2 q_y\\ -K^o_1 q^2 - K^o_2 & 0 & -iK^o_2 q_x\\ iK^o_2 q_y & -iK^o_2 q_x & 0\end{pmatrix}.$$

When $\rho > 0$, the allowed complex frequencies $\underline{\omega}$, solutions of Eq. (25), can be expressed in terms of the eigenvalues λ of $\mathcal{M}$ as

$$\underline{\omega}_\pm = -\frac{i}{2}\left[\frac{\Gamma}{\rho} \pm i\sqrt{\frac{48\lambda}{h^2\rho} - \frac{\Gamma^2}{\rho^2}}\right]. \tag{27}$$

In general, $\underline{\omega} = \omega + i\sigma$ are complex numbers: their real part ω is the (angular) frequency, while their imaginary part σ

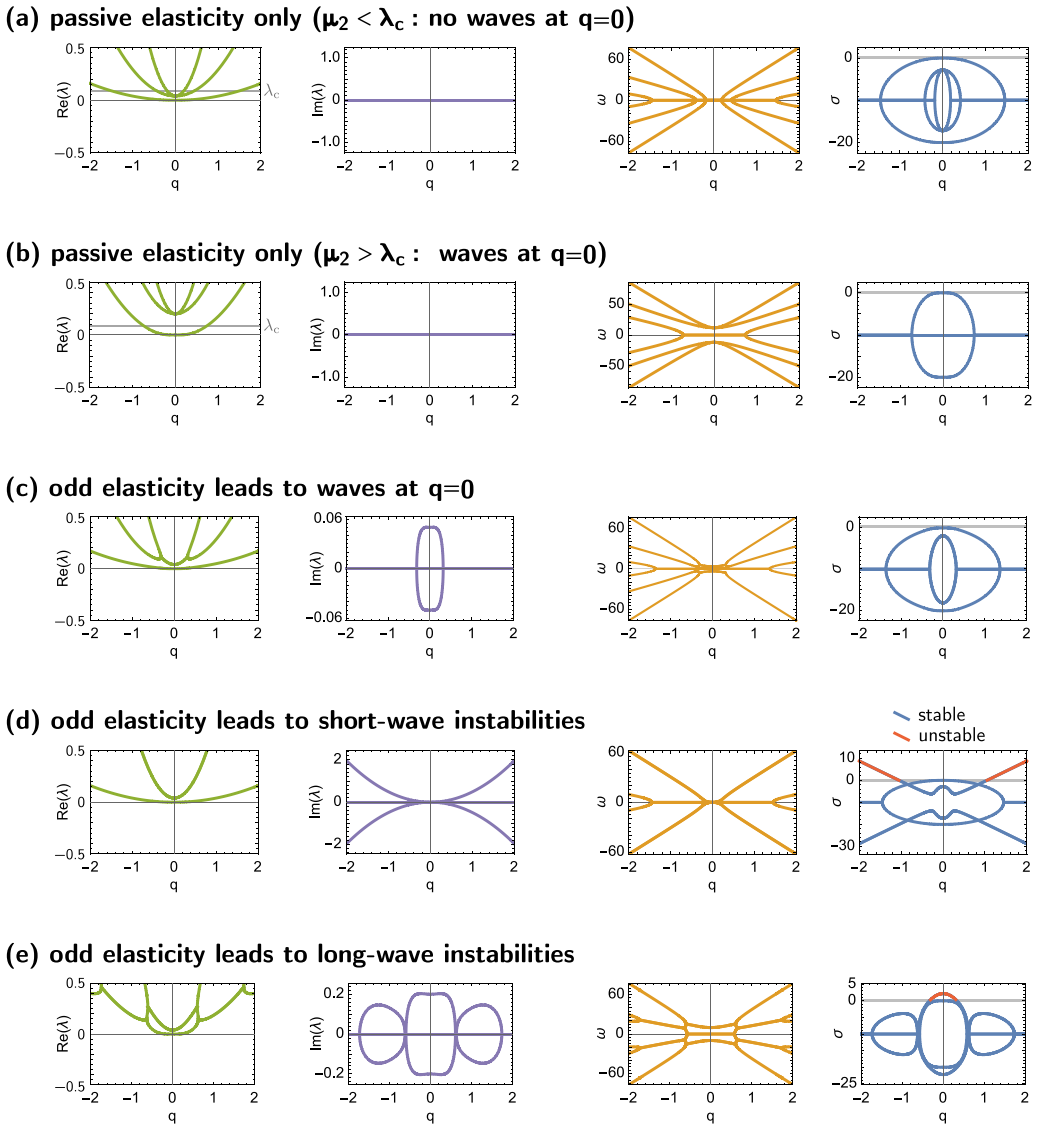

FIG. 4. Effect of odd elasticity of the dispersion relation. We plot the eigenvalues λ in Eq. (25) and the corresponding (angular) frequency ω and growth rate σ obtained from Eq. (26) in different cases. We have used the parameters $h = 0.1$, $\rho = 1$, $\Gamma = 20$, $B = 1$ in all panels. In addition, we have set (a) $\mu_1 = 0.25$, $\mu_2 = 0.04$, $K_1^o = 0$, $K_2^o = 0$, (b) $\mu_1 = 0.5$, $\mu_2 = 0.2$, $K_1^o = 0$, $K_2^o = 0$, (c) $\mu_1 = 0.25$, $\mu_2 = 0.04$, $K_1^o = 0$, $K_2^o = 0.05$, (d) $\mu_1 = 0.25$, $\mu_2 = 0.04$, $K_1^o = 0.7$, $K_2^o = 0$, (e) $\mu_1 = 0.25$, $\mu_2 = 0.04$, $K_1^o = 0$, $K_2^o = 0.2$.

is the growth rate of perturbations. In our convention $\sigma < 0$ indicates that perturbations decay and $\sigma > 0$ indicates that perturbations grow, a sign of instability. The spectrum of the dynamical matrix $\mathcal{M}$ depends only on $q = |\mathbf{q}|$ because of the cylindrical isotropy of the constitutive relations. It contains three bands in the complex plane, symmetric under reflection with respect to the real axis.

When odd elastic moduli vanish, the dynamical matrix $\mathcal{M}$ is Hermitian and therefore has real eigenvalues $\mu_2 + \mu_1 q^2$ and $X \pm \sqrt{X^2 - \mu_2(B+\mu_1)q^4}$ with $X = [\mu_2 + (B + \mu_1 + \mu_2)q^2]/2$. When μ_1, μ_2, and B are positive, these eigenvalues are also positive, and the growth rates are negative, which means that the system is linearly stable (except for two marginal modes at $q = 0$ that correspond to rigid body motions). When $\lambda < \lambda_c \equiv h^2\Gamma^2/(48\rho)$, the frequency ω vanishes: perturbations are overdamped. In particular, perturbations with $q \to 0$ are overdamped whenever $\mu_2 < \lambda_c$ [Figs. 4(a) and 4(b)].

When odd elastic moduli are nonzero, the dynamical matrix becomes non-Hermitian. When $\mathbf{q} = \mathbf{0}$, the dynamical matrix reduces to

$$\mathcal{M}(\mathbf{q} = 0) = \begin{pmatrix} \mu_2 & K_2^o & 0 \\ -K_2^o & \mu_2 & 0 \\ 0 & 0 & 0 \end{pmatrix}. \tag{28}$$

The eigenvalues of $\mathcal{M}(\mathbf{q} = 0)$ are $\lambda_\pm = \mu_2 \pm iK_2^o$ and $\lambda_0 = 0$. Hence, odd elastic moduli can induce (damped) oscillations at $q \to 0$ in an originally overdamped system, in a way similar to 2D odd elasticity [25]. More precisely, an arbitrarily small K_2^o does so when $\mu_2 < \lambda_c$ [Fig. 4(c)].

In addition, odd elastic moduli can induce linear instabilities: K_2^o tends to induce instabilities at $q = 0$ (because it couples to cross-sectional shearing), while K_1^o tends to induce

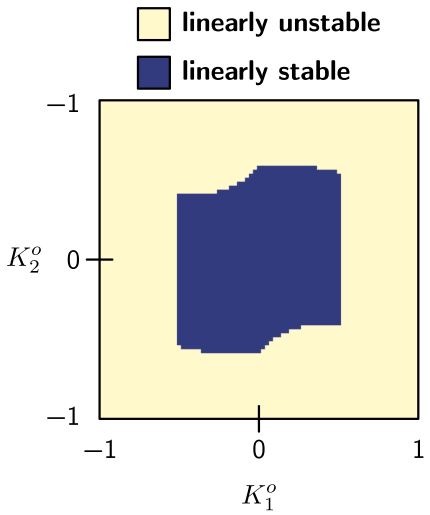

FIG. 5. Odd elasticity induces instabilities. We have used $h = 0.1$, $\rho = 1.0$, $\Gamma = 20.0$, $B = 1.0$, $\mu_1 = 1.0$, $\mu_2 = 1.0$.

instabilities at large q (because it couples to bending); see Figs. 4(d) and 4(e). This is illustrated in Fig. 5, in which we plot the regions in parameter space in which the system is linearly stable (i.e., $\sigma < 0$ for all $q > 0$) or unstable. For the parameters chosen, we observe that high enough odd elastic moduli always lead to instabilities. A second important case is the limit in which $\rho = 0$, wherein the frequencies are given by

$$\underline{\omega} = -i\frac{12\Gamma}{h^2}\lambda. \tag{29}$$

In this case the membrane is always stable ($\sigma < 0$) so long as $\tilde{B}$, μ_1, $\mu_2 > 0$. When B, μ_1, $\mu_2 = 0$, then $\underline{\omega}$ is entirely real (since $\mathcal{M}^o$ is anti-Hermitian), and so waves propagate without attenuation in this limit.

To summarize, odd elastic moduli have qualitative effects on the dispersion relation and modes of vibration of a moderately thick membrane: they affect wave propagation in the membrane, as well as its linear stability. This suggests that shape instabilities and oscillations predicted in active membranes [18,19,22,23,57,58] may be affected by the presence of odd elasticity, which should therefore be taken into account in order to describe living and robotic tissues.

B. Unidirectional edge states and bulk topology

Up to this point, we have focused on the bulk properties of the system, that correspond to the vibrational modes of an infinite, unbounded plate. These properties are contained in the eigenvalues and eigenvectors of $\mathcal{M}(\mathbf{q})$. We now utilize the topological properties of these bulk eigenvectors to show that unidirectional edge states may appear at the boundary of a finite plate (subject to appropriate boundary conditions). To do so, we first note that the spectrum of $\mathcal{M}(\mathbf{q})$ has a gap when odd elastic moduli are present: Fig. 6 shows that the spectrum consists of two gapped modes whose deformation is dominated by cross-sectional shearing. When the odd moduli are nonzero but sufficiently small [Figs. 6(c) and 6(d)], the spectrum has a nonzero imaginary part, but the gap is still sorted by the real (blue) part of the spectrum. By contrast, for sufficiently large K_2^o/μ_2, the gap opens in the imaginary part of the spectrum [Figs. 6(e) and 6(f)]. Finally, when the even moduli vanish, the spectrum is entirely imaginary [Figs. 6(g) and 6(h)]. When the gap is in the imaginary part, the chiral modulus K_2^o dominates over μ_2, and hence we may intuitively expect chiral phenomenology in the wave mechanics.

The reason for this band gap is the finite thickness h of the beam. Recall that plane waves in a 3D solid are described by a wave vector with three components (q_x, q_y, q_z). Since the plates we consider are thin the z direction, the minimum nonzero value of q_z is proportional to $1/h$, resulting in finite frequency modes even when $q_x = q_y = 0$. This gap is proportional to the moduli μ_2 and K_2^o because these moduli respond to cross-sectional shearing, which involves gradients in the z direction [cf. Eq. (15) and Table I]. Accordingly, the frequencies in (25) and (27) depend on the eigenvalues λ as $\rho\omega^2 + i\Gamma\omega \propto \lambda/h^2$. As $h \to 0$, the gapped cross-sectional shearing modes are pushed to arbitrarily high frequencies regardless of wave number. For sufficiently small h, the hydrodynamic description is no longer valid, and the theory is purely 2D and gapless, as considered in Ref. [19] and described by Eq. (23).

We now show that when the gap is open at sufficiently large K_2^o, the combination of chirality and a band gap gives rise to a nonzero topological invariant known as the Chern number, which leads to unidirectional wave propagation at the boundary of a finite system. In Appendix E we compute a topological invariant known as the first Chern number. This quantity can be expressed as the integral of the so-called Berry curvature over the momentum space. In most applications of topological band theory, the structure under consideration takes the form of a discrete lattice, and so the momentum space is a compact manifold (namely, a torus). By contrast, here we analyze continuum equations for which the momentum space corresponds to the real plane. This introduces additional subtleties regarding meaning and interpretation of the Chern number [53–56,59–63]. These aspects have been studied in the context of fluids with broken microscopic time-reversal and parity symmetries exhibiting a property known as odd viscosity [64]. In Appendix G we provide an explicit mapping between the odd-elastic plate and these fluids. Other (distinct) topological properties that have been studied in elastic continua include topological softness associated with floppy mechanisms in the microstructure [44,45].

For simplicity, in the main text we concentrate on the simplest scenario in which the bands are gapped is the purely active plate, where all even moduli vanish ($\tilde{B} = \mu_1 = \mu_2 = 0$). In this case the dynamical matrix reads

$$\mathcal{M}(\mathbf{q}) = \begin{pmatrix} 0 & K_1^o q^2 + K_2^o & iK_2^o q_y \\ -K_1^o q^2 - K_2^o & 0 & -iK_2^o q_x \\ iK_2^o q_y & -iK_2^o q_x & 0 \end{pmatrix}, \tag{30}$$

which has a flat band of eigenvalues $\lambda_0(q) = 0$ and two purely imaginary bands

$$\lambda_\pm(q) = \pm i\sqrt{\left(K_2^o q\right)^2 + \left(K_1^o q^2 + K_2^o\right)^2}. \tag{31}$$

The spectrum has a gap whenever $K_2^o \neq 0$. As detailed in Appendix E, if $K_1^o \neq 0$ the eigenvectors of $\mathcal{M}(\mathbf{q})$ do not

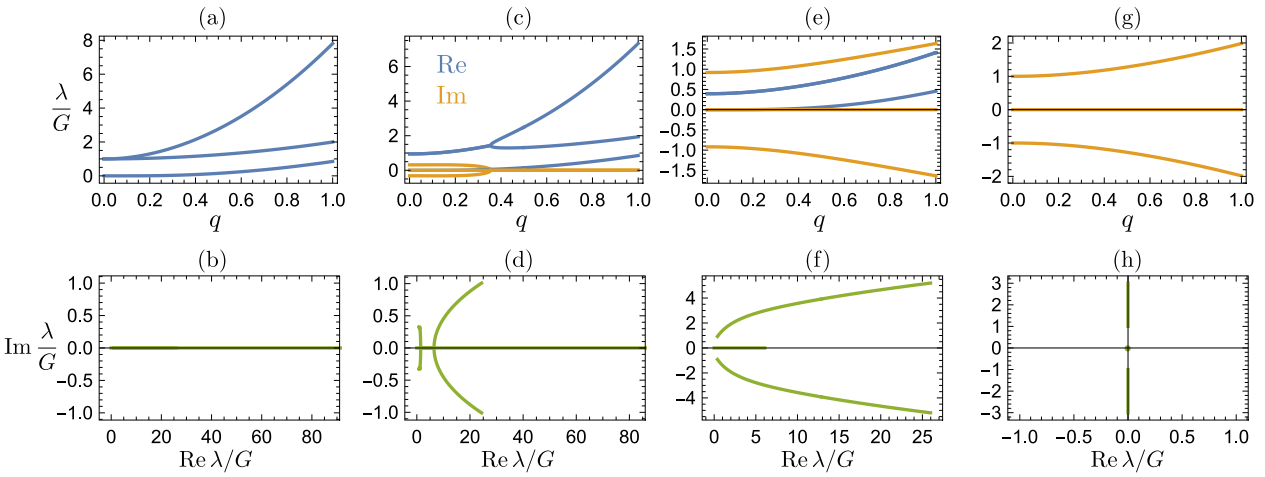

FIG. 6. Eigenvalues of the dynamical matrix in the complex plane. In (a), (c), (e), and (g) we plot real and imaginary part of the spectrum, and in (b), (d), (f), and (h) we plot the spectrum parametrically in the complex plane for $q \in [0, 5]$. The eigenvalues are expressed in units of $G = \sqrt{\mu_2^2 + K_2^{o2}}$. In (a) and (b) the odd moduli are zero and thus the spectrum is real. $\tilde{B}/G = 5.7$, $\mu_1/G = 1$, $\mu_2/G = 1$, $K_1^o/G = 0.0$, $K_2^o/G = 0.0$. In (c) and (d) the odd modules are turned on and the spectrum shows an imaginary part. $\tilde{B}/G = 5.4$, $\mu_1/G = 0.95$, $\mu_2/G = 0.95$, $K_1^o/G = 0.3$, $K_2^o/G = 0.3$. Lowering the (passive) bulk modulus and raising the odd moduli in (e) and (f), the spectrum becomes gapped. $\tilde{B}/G = 1.3$, $\mu_1/G = 0.4$, $\mu_2/G = 0.4$, $K_1^o/G = 0.66$, $K_2^o/G = 0.92$. In (g) and (h) the spectrum is completely imaginary as only the odd moduli are nonzero. $K_1^o/G = 0.7$, $K_2^o/G = 1$.

depend of the direction of $\mathbf{q}$ in the limit $\mathbf{q} \to \infty$. This allows us to compactify the momentum space to a sphere, identifying all the points at infinity. It is then possible to associate a topological invariant to the bulk eigenvectors associated with each band, the first Chern number $\mathcal{C}$. Its values are (see Appendix E)

$$\begin{aligned} \mathcal{C}_0 &= 0, \\ \mathcal{C}_+ &= \mathrm{sgn}K_2^o - \mathrm{sgn}K_1^o, \\ \mathcal{C}_- &= -\mathcal{C}_+. \end{aligned} \tag{32}$$

The presence of nonzero Chern numbers suggests that edge modes could appear at the system boundary [65]. In the continuum, the precise boundary conditions play a subtle role in determining the number of edge modes [55,56].

To illustrate the existence of the localized edge mode, we perform a numerical simulation of Eqs. (21) and (22) in the overdamped limit $\rho = 0$; see Fig. 7. We consider a finite plate that has its midplane defined over a region with boundary $\mathcal{B}$ and assume that the displacement field vanishes at the boundary:

$$w|_{\mathcal{B}} = 0, \quad \phi_x|_{\mathcal{B}} = 0, \quad \phi_y|_{\mathcal{B}} = 0. \tag{33}$$

In the top row (a–c) of Fig. 7, we have taken $K_1^o/K_2^o > 0$, which implies that the gapped vibrational bands are topologically trivial [$C_+ = 0$ in (32)]. Accordingly, when the membrane is periodically forced near its boundary, the deformation remains localized. By contrast, in the bottom row (d–f), we have taken $K_1^o/K_2^o > 0$, which implies that the gapped vibrational bands are topologically nontrivial [$C_+ = 2$ in (32)], and accordingly the system displays a unidirectional edge mode confined to its boundary. See Appendix F for details of the numerics and Supplemental Videos 1 and 2 [73] for full renderings of the simulations.

Finally, we comment that our analysis relies on the Reissner-Mindlin theory of thin plates. This theory is applicable for low-frequency modes. Hence, our analysis is valid only when the band gap is small enough to lie within the range of validity of the low frequency approximation. The precise range of validity often requires experimentation, but is generally larger for floppier materials with a lower shear modulus.

IV. CONCLUSION

In this work we studied the equations of motion for an odd-elastic plate in the Reissner-Mindlin moderately thick limit. The in-plane dynamics of the plate follows the equations of 2D odd elasticity. The out-of-plane dynamics displays additional odd elastic responses. We have shown that the dispersion relation and normal modes are qualitatively affected by odd elasticity, which can induce linear instabilities and affect wave propagation in the plate. We have also shown that the spectrum is gapped as long as the active elastic moduli are dominant with respect to the passive ones. Moreover, the bands can acquire a nonzero Chern number, and this leads to the emergence of unidirectional waves at the boundary of a finite plate. In more complex geometries, odd elastic responses may also affect shape instabilities and self-actuation in active membranes.

The continuum theory developed in this work may serve as a guide to design active mechanical metamaterials with desired waveguide properties, for instance, using piezoelectric materials [28]. All that is generically required is the breaking of 2D chirality, effective nonconservative forces that depend on strain, and a geometry consisting of a moderately thick cross section. Possible extensions of our analysis include frequency-dependent (i.e., viscoelastic) moduli [26,66–68],

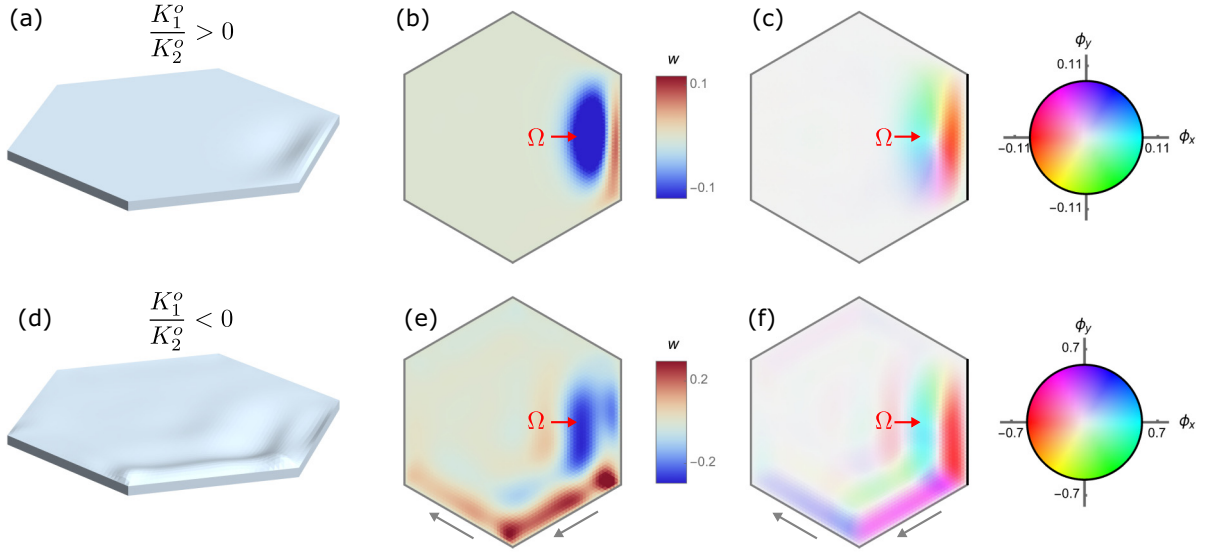

FIG. 7. Simulation of topological edge mode. A numerical solution to Eqs. (21) and (22) with $K_1^o/K_2^o > 0$ (a)–(c) and $K_1^o/K_2^o < 0$ (d)–(f). Panels (a) and (d) are 3D renderings, panels (b) and (d) show the height field w, and panels (c) and (f) depict $\boldsymbol{\phi}$. The red arrows (b), (c), (e), (f) indicate the location of the driving, and the gray arrows (e), (f) indicate the direction of wave propagation. When $K_1^o/K_2^o > 0$, the gapped vibrational bands are topologically trivial [$C_+ = 0$ in Eq. (32)]. When $K_1^o/K_2^o < 0$, the gapped bands are topologically nontrivial [$C_+ = 2$ in Eq. (32)], resulting in a boundary mode. See Appendix F for details of the numerics, including nondimensionalization of the variables. In all panels the nondimensionalized moduli are $\tilde{K}_2^o = 2$, $\tilde{\mu}_2 = 0.05$, $\tilde{B} = 0$, $\tilde{\mu}_1 = 0$, while $\tilde{K}_1^o = 1$ in (a)–(c) and $\tilde{K}_1^o = -1$ in (d)–(f). The membrane is driven near its right boundary at a frequency $\tilde{\Omega} = 0.1$. See Supplemental Movies 1 and 2 [73] for renderings of the full simulations.

the role of background curvature, and odd elasticity coupled with other effects such as flows [19,20]. Beyond artificial systems, shape sensing and active stresses naturally occur in biological media such as membranes with protein pumps [69,70], the actomyosin cortex [71], macroscopic tissues [72], or rafts of living organisms [31]. The nonconservative mechanics of odd membranes may provide a lens to interpret naturally occurring dynamics, or control biosynthetic media.

The computer code used in this study is available on Zenodo at [74] under the 2-clause BSD licence.

ACKNOWLEDGMENTS

M.Fo. would like to thank L. Molinari for fruitful conversation. C.S. acknowledges support from the Bloomenthal Fellowship and the National Science Foundation Graduate Research Fellowship under Grant No. 1746045. M.Fr. acknowledges support from the National Science Foundation under Grant No. DMR-2118415, a Kadanoff-Rice fellowship funded by the National Science Foundation under Award No. DMR-2011854 and the Simons Foundation. V.V. acknowledges support from the Army Research Office under Grants No. W911NF-22-2-0109 and No. W911NF-23-1-0212. M.Fr. and V.V acknowledge support from the France Chicago center through a FACCTS grant. This research was supported from the National Science Foundation through the Center for Living Systems (Grant No. 2317138).

APPENDIX A: ODD ELASTIC MODULI IN THREE DIMENSIONS WITH CYLINDRICAL SYMMETRY

Odd elasticity cannot arise in systems with spherical isotropy (i.e., invariance under all rotations in three dimensions). However, it can arise in systems with cylindrical isotropy (i.e., invariance under all rotations preserving the z axis) [25]. In this Appendix we construct the most general elastic tensor in a bulk 3D system with cylindrical symmetry, i.e., a rank-four tensor which does not change when the coordinate system is rotated around the z axis. Since both the strain and the stress are symmetric, we introduce a basis for symmetric rank 2 tensors $\mathcal{G} = \{g^0, \ldots, g^5\}$ by

$$g^0_{ij} = \frac{1}{\sqrt{3}}\begin{pmatrix}1&0&0\\0&1&0\\0&0&1\end{pmatrix}, \qquad g^1_{ij} = \frac{1}{\sqrt{6}}\begin{pmatrix}-1&0&0\\0&-1&0\\0&0&2\end{pmatrix}, \tag{A1a}$$

$$g^2_{ij} = \frac{1}{\sqrt{2}}\begin{pmatrix}1&0&0\\0&-1&0\\0&0&0\end{pmatrix}, \qquad g^3_{ij} = \frac{1}{\sqrt{2}}\begin{pmatrix}0&1&0\\1&0&0\\0&0&0\end{pmatrix}, \tag{A1b}$$

$$g^4_{ij} = \frac{1}{\sqrt{2}}\begin{pmatrix}0&0&1\\0&0&0\\1&0&0\end{pmatrix}, \qquad g^5_{ij} = \frac{1}{\sqrt{2}}\begin{pmatrix}0&0&0\\0&0&1\\0&1&0\end{pmatrix}. \tag{A1c}$$

In this Appendix Greek labels refer to the element of the basis $\mathcal{G}$ in Eq. (A1). Notice that $\mathcal{G}$ can be decomposed into irreducible representations of SO(3): g^0 lies in the trivial representation, and $g^1, \ldots, g^5$ (symmetric traceless matrices) lie

in a "spin 2" irreducible representation. The basis is orthonormal with respect to the trace scalar product $\langle a, b\rangle = \mathrm{tr}(ab)$. Hence, an arbitrary symmetric tensor t_{ij} can be decomposed as $t_{ij} = \sum_\alpha t_\alpha g^\alpha_{ij}$ with

$$t_\alpha = \sum_{ij} t_{ij} g^\alpha_{ij}. \tag{A2}$$

The elastic tensor is a linear operator over the space of rank two tensors, and its representative matrix can be calculated by

$$C_{\alpha\beta} = \sum_{ijk\ell} g^\alpha_{ij} C_{ijk\ell} g^\beta_{k\ell}. \tag{A3}$$

Hooke's law can thus be expressed as

$$\sigma_\alpha = \sum_\beta C_{\alpha\beta} u_\beta. \tag{A4}$$

Under a rotation r of the reference system, the matrix g^α changes into $g'^\alpha = r g^\alpha r^{\mathrm{t}}$ (t denotes transposition). Since g'^α is also symmetric, it can be decomposed on the $\mathcal{G}$ basis, defining the representation of rotations R over the rank-two tensors: $g'^\alpha_{ij} = R^{\alpha\beta} g^\beta_{ij}$. Under rotations, the elastic modulus tensor transforms as $C'_{\alpha\beta} = R^{\alpha\mu} C_{\mu\nu} (R^{\mathrm{t}})^{\nu\beta}$. Cylindrical isotropy means that C is invariant under rotations about the z axis, i.e., $C = RCR^{\mathrm{t}}$. Equivalently, C commutes with the representation of the generator of rotations about the z axis, L_z, which is given by

$$L_z = \begin{pmatrix} 0 & 0 & 0 & 0 & 0 & 0 \\ 0 & 0 & 0 & 0 & 0 & 0 \\ 0 & 0 & 0 & 2 & 0 & 0 \\ 0 & 0 & -2 & 0 & 0 & 0 \\ 0 & 0 & 0 & 0 & 0 & 1 \\ 0 & 0 & 0 & 0 & -1 & 0 \end{pmatrix}. \tag{A5}$$

Imposing $[C, L_z] = 0$, one finds that the most general elastic tensor with cylindrical isotropy reads

$$C_{3\mathrm{D}} = 2\begin{pmatrix} \frac{3}{2}B & D+H & 0 & 0 & 0 & 0 \\ D-H & \mu_3 & 0 & 0 & 0 & 0 \\ 0 & 0 & \mu_1 & K_1^o & 0 & 0 \\ 0 & 0 & -K_1^o & \mu_1 & 0 & 0 \\ 0 & 0 & 0 & 0 & \mu_2 & K_2^o \\ 0 & 0 & 0 & 0 & -K_2^o & \mu_2 \end{pmatrix}. \tag{A6}$$

Here B is the bulk modulus, which couples spherically symmetric dilations to pressure, μ_1, μ_2, μ_3 are shear moduli, which couple shear deformations to the corresponding shear stress, and D is a passive mixed modulus that couples passively the cylindrically symmetric shear strain to pressure and spherically symmetric dilations to cylindrically symmetric stress. The modulus H is the antisymmetric (or odd) counterpart of the modulus D. The modulus K_1^o is an antisymmetric coupling between shears 2 and 3 in the x-y plane, while K_2^o is an antisymmetric coupling between shears 4 and 5, which could be respectively called xz and yz shears. In three dimensions, one can show that an isotropic [i.e., SO(3)-symmetric] elastic tensor cannot contain odd elastic moduli [25].

TABLE II. Comparison between all moduli compatible with planar isotropy and those obtained from a 3D bulk material. Mixed coefficients may be replaced with even and odd combinations (for instance, $C_{30} + C_{03}$ is even while $C_{30} - C_{03}$ is odd).

Planar isotropy Eq. (B5)	Limit of 3D material Eqs. (13)–(15)	Even or odd
C_{00}	$2h\tilde{B}$	Even
C_{11}	$2h\mu_1$	Even
C_{12}	$2hK_1^o$	Odd
C_{03}	0	Mixed
C_{14}	0	Mixed
C_{15}	0	Odd
C_{33}	$(h^3/6)\tilde{B}$	Even
C_{44}	$(h^3/6)\mu_1$	Even
F_{PC}	$(h^3/6)K_1^o$	Odd
C_{30}	0	Mixed
C_{41}	0	Mixed
C_{42}	0	Odd
C_{66}	$2h\mu_2$	Even
C_{67}	$2hK_2^o$	Odd

APPENDIX B: PLATE CONSTITUTIVE RELATIONS

Directly from the parameterization of the displacement field in the plate, and thus from the kinematic assumptions on the allowed displacements, we have that u_{zz} vanishes identically. Then its conjugate variable, the vertical stress σ_{zz}, does not affect the dynamics, and it is common practice [12] to set it to zero—imposing the so-called *plane-stress condition*. The constitutive relations of the bulk 3D material with cylindrical isotropy [Eq. (A6)] are modified by this assumption, and a reduced elastic tensor for the plate, which maps the nonzero strains into the nonzero stresses, is calculated.

To do so, we decompose the stress vector $\sigma^{3\mathrm{D}} = (\sigma_0, \ldots, \sigma_5) = (\sigma_Z, \sigma_{/\!/})$ into a in-plane component $\sigma_{/\!/} = (\sigma_1, \ldots, \sigma_4)$ and an out-of-plane component $\sigma_Z = \sigma_0$, and similarly for the strain vector $u^{3\mathrm{D}} = (u_Z, u_{/\!/})$. Here the components σ_a and u_a of the stress and strain vector refer to the basis vectors B^a defined in Eq. (7). The elastic matrix $C^{3\mathrm{D}}$ in the bulk constitutive relation (A6) can then be seen as a block matrix:

$$\begin{pmatrix} \sigma_Z \\ \sigma_{/\!/} \end{pmatrix} = C^{3\mathrm{D}} \begin{pmatrix} u_Z \\ u_{/\!/} \end{pmatrix} = \begin{pmatrix} C_{ZZ} & C_{Z/\!/} \\ C_{/\!/Z} & C_{/\!//\!/} \end{pmatrix} \begin{pmatrix} u_Z \\ u_{/\!/} \end{pmatrix}. \tag{B1}$$

Note that the matrix in Eq. (A6) is written in the basis (A1), while Eq. (B1) is written in the basis (7). A change of basis matrix has to be applied to Eq. (A6) before carrying out the procedure delineated here.

Assuming $\sigma_Z = 0$, solving for u_Z (leading to $u_Z = -C_{ZZ}^{-1} C_{Z/\!/} u_{/\!/}$) and replacing, we find

$$\sigma_{/\!/} = C^{\text{eff}} u_{/\!/} \qquad \text{where} \qquad C^{\text{eff}} = C_{/\!//\!/} - C_{/\!/Z} C_{ZZ}^{-1} C_{Z/\!/}. \tag{B2}$$

In the main text, we use the simplified notations $\sigma \equiv \sigma_{/\!/}$ and $C \equiv C^{\text{eff}}$.

Using the constitutive relation (A6) for the 3D bulk, this leads to

$$C_{ab} \equiv C_{ab}^{\text{eff}} = 2 \begin{pmatrix} \tilde{B} & 0 & 0 & 0 & 0 \\ 0 & \mu_1 & K_1^o & 0 & 0 \\ 0 & -K_1^o & \mu_1 & 0 & 0 \\ 0 & 0 & 0 & \mu_2 & K_2^o \\ 0 & 0 & 0 & -K_2^o & \mu_2 \end{pmatrix} \tag{B3}$$

with

$$\tilde{B} = \frac{-6D^2 + 6H^2 + 9B\mu_3}{3B + 4(\sqrt{2}D + \mu_3)}. \tag{B4}$$

Notice that $\tilde{B}$ is a nontrivial function of the 3D bulk modulus B, 3D axial shear modulus μ_3, as well as the moduli D and H which relate 3D dilations and axially symmetric shear in a symmetric and antisymmetric way, respectively (see Appendix A for more details). In contrast, the remaining shear moduli are inherited in a straightforward way from three dimensions.

More generally, we can consider moduli that are consistent with planar isotropy but do not arise from the thin limit of a 3D structure. The constitutive relation in this case takes the more general form

$$\begin{pmatrix} N_D \\ N_{S^1} \\ N_{S^2} \\ M_D \\ M_{S^1} \\ M_{S^2} \\ N_{T^x} \\ N_{T^y} \end{pmatrix} = \begin{pmatrix} C_{00} & 0 & 0 & C_{03} & 0 & 0 & 0 & 0 \\ 0 & C_{11} & C_{12} & 0 & C_{14} & C_{15} & 0 & 0 \\ 0 & -C_{12} & C_{11} & 0 & -C_{15} & C_{14} & 0 & 0 \\ C_{30} & 0 & 0 & C_{33} & 0 & 0 & 0 & 0 \\ 0 & C_{41} & C_{42} & 0 & C_{44} & C_{45} & 0 & 0 \\ 0 & -C_{42} & C_{41} & 0 & -C_{45} & C_{44} & 0 & 0 \\ 0 & 0 & 0 & 0 & 0 & 0 & C_{66} & C_{67} \\ 0 & 0 & 0 & 0 & 0 & 0 & -C_{67} & C_{66} \end{pmatrix} \begin{pmatrix} u_D^0 \\ u_{S^1}^0 \\ u_{S^2}^0 \\ u_D^1 \\ u_{S^1}^1 \\ u_{S^2}^1 \\ u_{T^x}^0 \\ u_{T^y}^0 \end{pmatrix} \tag{B5}$$

to be compared with Eqs. (13)–(15). In Eq. (B5) the coefficients in red (namely, $C_{03}, C_{14}, C_{15}, C_{30}, C_{41}, C_{42}$) do not arise from the thin limit of a 3D structure. A comparison between the plates' elastic moduli in Eq. (B5) and in Eqs. (13)–(15) is given in Table II.

APPENDIX C: RELATION WITH THE NOTATIONS OF SALBREUX *ET AL.*

In this Appendix we compare our notation to that of Ref. [19], which considers active membrane mechanics in the limit $h \to 0$. In our notation we use Greek letters for in-plane indices, and we do not distinguish between up and down indices since we linearize about a flat membrane. In our notation (their notation), the in-plane stress tensor is denoted $N_{\alpha\beta}$ (t^{ij}), the linearized 2D strain tensor is denoted $u_{\alpha\beta}$ (u^{ij}), the in-plane bending moment is denoted $M_{\alpha\beta}$ ($\bar{m}^{ij}$), and midplane curvature is denoted $\partial_\alpha \partial_\beta \omega$ (c^{ij}). Using the notation of Eq. (B5) in our work and Eqs. (66) and (67) in Ref. [19], we can also compare the elastic moduli: this is done in Table III. We note that C_{66} and C_{67} do not appear in Ref. [19] because these terms couple explicitly to the finite thickness degree of freedom ϕ, which is not studied in the $h \to 0$ limit. Likewise, the elastic coefficients $H_1, \bar{H}_1, \bar{H}_2, H_C, \bar{H}_C$, and H_{PC} in Refs. [19] do not appear in our work as they are coefficients of a geometric term Ω_i which involves background curvature and higher-order gradients of the displacement field not considered in the present work.

TABLE III. Comparison of the notations used in this work and the notations of Ref. [19]. The coefficients C_{66} and C_{67} do not appear in Ref. [19] because these terms couple explicitly to the finite thickness degree of freedom ϕ, which is not studied in the $h \to 0$ limit. Likewise, the elastic coefficients $H_1, \bar{H}_1, \bar{H}_2, H_C, \bar{H}_C$, and H_{PC} in Ref. [19] do not appear in our work because they are coefficients of a geometric term Ω_i which involves background curvature and higher-order gradients of the displacement field not considered in the present work. See Table II for a correspondence with the notations used in the main text.

	This work	Ref. [19]
In-plane stress tensor	$N_{\alpha\beta}$	t^{ij}
In-plane bending moment	$M_{\alpha\beta}$	$\bar{m}^{ij}$
Midplane curvature	$\partial_\alpha \partial_\beta \omega$	c^{ij}
Elastic coefficients	C_{00}	$E_2 + E_1/2$
	C_{11}	$E_1/2$
	C_{12}	E_{PC}
	C_{03}	$G_2 + G_1/2$
	C_{14}	$G_1/2$
	C_{15}	G_C
	C_{33}	$F_2 + F_1/2$
	C_{44}	$F_1/2$
	F_{PC}	C_{45}
	C_{30}	$K_2 + K_1/2$
	C_{41}	$K_1/2$
	C_{42}	$-K_C$
	C_{66}	n/a
	C_{67}	n/a

APPENDIX D: DERIVATION OF THE EQUATIONS OF MOTION AND EXPLICIT $h \to 0$ LIMIT

In this Appendix we calculate the equations describing the evolution of the plate in the bulk using the principle of virtual work. We consider a plate that is infinite along the x and y directions, and has finite thickness along $z \in [-h/2, h/2]$. The region occupied by the plate at rest is then $V = \mathbb{R}^2 \times [-h/2, h/2]$. The displacement field configurations are assumed to vanish at infinity. We consider an external drag force given by $f_i^{\text{ext}} = -\Gamma \dot{\xi}_i$.

The virtual work principle states that the actual field configuration in its time evolution from t_i to t_f must satisfy

$$\int_{t_i}^{t_f} dt(\delta K - \delta W^{\text{int}} - \delta W^{\text{ext}}) = 0, \tag{D1}$$

where K is the kinetic energy, δW^{int} is the internal infinitesimal work, and δW^{ext} is the external infinitesimal work, given by

$$K = \frac{1}{2}\int_V d^3x\, \rho \dot{\xi}_i \dot{\xi}_i, \quad \delta W^{\text{int}} = \int_V d^3x\, \sigma_{ij}\delta u_{ij}, \quad \delta W^{\text{ext}} = \int_V d^3x\, f_i^{\text{ext}} \delta \xi_i \tag{D2}$$

in which the variations δ are performed within the allowed displacements [12]. Notice that the principle of virtual work is valid even for nonconservative forces (like f^{ext} or odd elastic forces) because it requires only energy differential δW. While δW is integrated over space and time, allowing for integration by parts of spatiotemporal derivatives, it is not required to integrate δW over the variation of the fields to obtain an explicit potential W. When the explicit potential W exists (which is not required in the derivation below), the differential δ may be pulled outside of the space-time integral, and an action is obtained for a Lagrangian theory.

In the following, we express the 3D displacement field with respect to the plate fields, then we integrate over z, assuming a uniform density. The terms that survive are the ones that contain an even power of z. Finally we integrate by parts in order to isolate the variations of the fields. For the kinetic energy, we have

$$\begin{aligned}
\int_{t_i}^{t_f} dt\, \delta K &= \int_{t_i}^{t_f} dt \int_V d^3x\, \rho[(\dot{\eta}_\alpha + z\dot{\phi}_\alpha)\delta(\dot{\eta}_\alpha + z\dot{\phi}_\alpha) + \dot{w}\delta\dot{w}] \\
&= \int_{t_i}^{t_f} dt \int_{\mathbb{R}^2} d^2x\, \rho\left[h\dot{\eta}_\alpha\delta\dot{\eta}_\alpha + h\dot{w}\delta\dot{w} + \frac{h^3}{12}\dot{\phi}_\alpha\delta\dot{\phi}_\alpha\right] \\
&= -\int_{t_i}^{t_f} dt \int_{\mathbb{R}^2} d^2x\, \rho\left[h\ddot{\eta}_\alpha\delta\eta_\alpha + h\ddot{w}\delta w + \frac{h^3}{12}\ddot{\phi}_\alpha\delta\phi_\alpha\right].
\end{aligned} \tag{D3}$$

For the internal elastic forces, we have

$$\begin{aligned}
\int_{t_i}^{t_f} dt\, \delta W_{\text{int}} &= \int_{t_i}^{t_f} dt \int_V d^3x\, [\sigma_{\alpha\beta}(\partial_\alpha\delta\eta_\beta + z\partial_\alpha\delta\phi_\beta) + \sigma_{z\alpha}\delta\phi_\alpha + \sigma_{\alpha z}\partial_\alpha\delta w] \\
&= \int_{t_i}^{t_f} dt \int_{\mathbb{R}^2} d^2x\, [N_{\alpha\beta}\partial_\alpha\delta\eta_\beta + M_{\alpha\beta}\partial_\alpha\delta\phi_\beta + N_{z\alpha}\delta\phi_\alpha + N_{\alpha z}\partial_\alpha\delta w] \\
&= \int_{t_i}^{t_f} dt \int_{\mathbb{R}^2} d^2x\, [-\partial_\alpha N_{\alpha\beta}\delta\eta_\beta - \partial_\alpha M_{\alpha\beta}\delta\phi_\beta + N_{z\alpha}\delta\phi_\alpha - \partial_\alpha N_{\alpha z}\delta w].
\end{aligned} \tag{D4}$$

For the external forces, we have

$$\int_{t_i}^{t_f} dt\, \delta W_{\text{ext}} = \int_{t_i}^{t_f} dt \int_{\mathbb{R}^2} d^2x\, \Gamma\left[h\dot{\eta}_\alpha\delta\eta_\alpha + h\dot{w}\delta w + \frac{h^3}{12}\dot{\phi}_\alpha\delta\phi_\alpha\right]. \tag{D5}$$

Finally, requiring Eq. (D1) to be satisfied for all the variations of the plate's fields, we get

$$h(\rho\ddot{\eta}_\alpha + \Gamma\dot{\eta}_\alpha) = \partial_\beta N_{\beta\alpha}, \tag{D6}$$

$$h(\rho\ddot{w} + \Gamma\dot{w}) = \partial_\alpha N_{\alpha z}, \tag{D7}$$

$$\frac{h^3}{12}(\rho\ddot{\phi}_\alpha + \Gamma\dot{\phi}_\alpha) = \partial_\beta M_{\beta\alpha} - N_{z\alpha}. \tag{D8}$$

Substituting the constitutive relations we get Eqs. (20) to (22).

We now discuss the $h \to 0$ limit of Eqs. (21) and (22). Let L be a typical length scale over which the membrane deflects and treat $\varepsilon \equiv h/L$ as a small parameter. Let $D_t = \rho\partial_t^2 + \Gamma\partial_t$, and normalize the x coordinate by L. Then the equations of motion Eqs. (21) and (22) read

$$D_t w = \partial_\alpha\big[\big(\mu_2\delta_{\alpha\beta} + K_2^o\epsilon_{\alpha\beta}\big)(\partial_\beta w + \phi_\beta)\big], \tag{D9}$$

$$\begin{aligned}\epsilon^2 D_t\phi_\alpha =& \epsilon^2(B\partial_\alpha\partial_\beta + \mu_1\nabla^2\delta_{\alpha\beta} + K_1^o\nabla^2\epsilon_{\alpha\beta})\phi_\beta \\ &- 12(\mu_2\delta_{\alpha\beta} + K_2^o\epsilon_{\alpha\beta})(\partial_\beta w + \phi_\beta).\end{aligned} \tag{D10}$$

To understand the $\epsilon \to 0$ limit, we organize the fields as

$$w(x,t) = w^{(0)}(x,t) + \epsilon^2 w^{(2)}(x,t) + \cdots, \tag{D11}$$

$$\phi_\alpha(x,t) = \phi_\alpha^{(0)}(x,t) + \epsilon^2\phi_\alpha^{(2)}(x,t) + \cdots. \tag{D12}$$

To zeroth order in ϵ, Eq. (D10) implies that

$$\phi_\beta^{(0)} = -\partial_\beta w^{(0).} \tag{D13}$$

Plugging in Eq. (D13) into Eq. (D9) implies that $D_t w^{(0)} = 0$ and hence, by virtue of Eq. (D13), $D_t\phi_\alpha^{(0)} = 0$. Using the fact that $D_t\phi_\alpha^{(0)} = 0$, the ϵ^2 contribution to Eq. (D10) reads

$$\begin{aligned}&\big(\mu_2\delta_{\alpha\beta} + K_2^o\epsilon_{\alpha\beta}\big)\big(\partial_\beta w^{(2)} + \phi_\beta^{(2)}\big) \\ &\quad = \tfrac{1}{12}\big(B\partial_\alpha\partial_\beta + \mu_1\nabla^2\delta_{\alpha\beta} + K_1^o\nabla^2\epsilon_{\alpha\beta}\big)\phi_\beta^{(0)}.\end{aligned} \tag{D14}$$

Combining Eq. (D10) and Eq. (D13) yields

$$\partial_\alpha w^{(2)} + \phi_\alpha^{(2)} = -\frac{B\mu_2\partial_\alpha\partial_\beta + K_2^o B\epsilon_{\alpha\gamma}\partial_\gamma\partial_\beta + \big(\mu_1\mu_2 - K_1^oK_2^o\big)\delta_{\alpha\beta}\nabla^2 + \big(\mu_2K_1^o + K_2^o\mu_1\big)\nabla^2\epsilon_{\alpha\beta}}{12\Big[\mu_2^2 + \big(K_2^o\big)^2\Big]}\partial_\beta w^{(0)}. \tag{D15}$$

Plugging Eq. (D15) into the ϵ^2 contribution to Eq. (D9) yields

$$D_t w^{(2)} = \partial_\alpha\big[\big(\mu_2\delta_{\alpha\beta} + K_2^o\epsilon_{\alpha\beta}\big)\big(\partial_\beta w^{(2)} + \phi_\beta^{(2)}\big)\big] \tag{D16}$$

$$= -\frac{(B+\mu_1)\big[\mu_2^2 - \big(K_2^o\big)^2\big] - 2\mu_2K_1^oK_2^o}{12\Big[\mu_2^2 + \big(K_2^o\big)^2\Big]}\nabla^4 w^{(0)}. \tag{D17}$$

Therefore, the equation of motion for w is closed unto itself to leading order in h/L. In original units, it is given by the Kirchhoff-Love theory of plates

$$\big(\rho\partial_t^2 + \Gamma\partial_t\big)w = -D_{\text{eff}}\nabla^4 w, \tag{D18}$$

where D_{eff} is a bending stiffness whose value is renormalized by the odd moduli K_1^o and K_2^o

$$D_{\text{eff}} = h^2\frac{(B+\mu_1)\big[\mu_2^2 - \big(K_2^o\big)^2\big] - 2\mu_2K_1^oK_2^o}{12\Big[\mu_2^2 + \big(K_2^o\big)^2\Big]} \tag{D19}$$

with the constraint $\phi_\alpha = -\partial_\alpha w$.

APPENDIX E: CALCULATION OF THE FIRST CHERN NUMBER

Here we show that for a purely active plate, as long as $K_2^o, K_1^o \neq 0$, momentum space can be compactified to a sphere. Once momentum space is compactified, we may define the first Chern number as a topological invariant for the eigenvector bands, which is later calculated. The reader is directed to Ref. [54] and references therein for more details.

We write the purely active dynamical matrix as a linear combination of the matrices

$$S_x = \begin{pmatrix}0&0&0\\0&0&-1\\0&-1&0\end{pmatrix}, \quad S_y = \begin{pmatrix}0&0&1\\0&0&0\\1&0&0\end{pmatrix},$$
$$S_z = \begin{pmatrix}0&-i&0\\i&0&0\\0&0&0\end{pmatrix} \tag{E1}$$

with $\mathcal{M}(\mathbf{q}) = i\vec{M}(\mathbf{q})\cdot\vec{S}$, and $\vec{M}(\mathbf{q}) = (K_2^oq_x, K_2^oq_y, K_1^oq^2 + K_2^o)$. Since a multiplicative factor does not change the eigenvectors of a matrix, the Hamiltonian $\mathcal{N}(\mathbf{q}) = \hat{n}(\mathbf{q})\cdot\vec{S}$, with $\hat{n} = \vec{M}/||\vec{M}||$, has the same eigenvectors as $\mathcal{M}(\mathbf{q})$ and thus the properties of the bands of eigenvectors of $\mathcal{M}$ can be studied equivalently on $\mathcal{N}$. Explicitly, we have

$$\hat{n}(\mathbf{q}) = \frac{1}{\sqrt{q^2 + \big(1 + K_1^o/K_2^oq^2\big)^2}}\begin{pmatrix}q_x\\q_y\\(K_1^o/K_2^o)q^2 + 1\end{pmatrix}, \tag{E2}$$

which is well defined on the whole momentum space if $K_2^o \neq 0$. If in addition $K_1^o \neq 0$, then $\lim_{\mathbf{q}\to\infty}\hat{n}(\mathbf{q})$ does not depend on the chosen direction. Identifying all the points at infinity, we compactify the momentum space to a sphere. In this case the eigenvectors of each band form a vector bundle over a compact manifold and the first Chern number is a well-defined topological invariant.

The Berry curvature F of the bands of $\mathcal{M}$ coincides with the Berry curvature of the bands of $\mathcal{N}$, so we will focus on the latter. We define the following map from 3D unit vectors to 3×3 complex matrices

$$\begin{aligned}&\mathscr{S} : \mathbb{S}^2 \to \text{Mat}(3,\mathbb{C}),\\ &\hat{v} \mapsto \hat{v}\cdot\vec{S} = v_xS_x + v_yS_y + v_zS_z.\end{aligned} \tag{E3}$$

Then $\mathcal{N}$ is the composition of $\hat{n}$ and $\mathscr{S}$, i.e., $\mathcal{N} : \mathbb{R}^2 \xrightarrow{\hat{n}} \mathbb{S}^2 \xrightarrow{\mathscr{S}} \text{Mat}(3,\mathbb{C})$. Each band of eigenvectors of $\mathscr{S}$ induces a Berry curvature $F^{\mathbb{S}^2}$ on the sphere. The Berry curvature F induced by $\mathcal{N}$ is equal to the pull-back through $\hat{n}$ of $F^{\mathbb{S}^2}$, i.e., $F = \hat{n}^*F^{\mathbb{S}^2}$. The curvature $F^{\mathbb{S}^2}$ can be calculated explicitly as follows. Let $\hat{n} = (\sin\theta\cos\phi, \sin\theta\sin\phi, \cos\theta)$, the eigenvectors of the positive and negative bands of $\mathcal{N} = \hat{n}\cdot\vec{S}$ are

$$\psi_\pm(\hat{n}) = \frac{1}{\sqrt{2}}\begin{pmatrix}\cos\theta\cos\phi \mp i\sin\theta\\ \pm i\cos\phi + \cos\theta\sin\phi\\ -i\sin\theta\end{pmatrix}. \tag{E4}$$

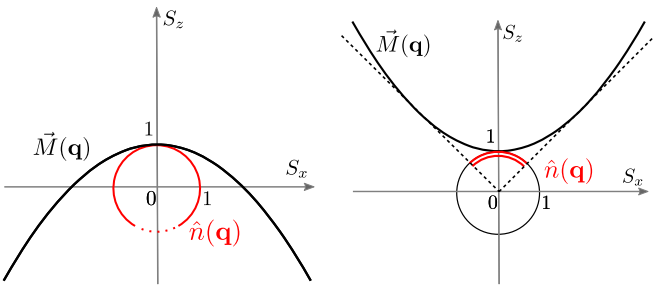

(a) $K_1^o/K_2^o < 0$. (b) $K_1^o/K_2^o > 0$.

FIG. 8. Visualization of Chern number calculation A cross section of $\vec{M}(\mathbf{q})$ and $\hat{n}(\mathbf{q})$ shows the index of the maps. In red, the projection on the unit sphere. The behavior of the map $\hat{n}$ can be understood visualizing the map $\vec{M}$. (a) $\vec{M}$ describes a paraboloid that encloses the origin, then $\hat{n} = \vec{M}/||\vec{M}||$ covers the whole unit sphere. (b) $\vec{M}$ describes a paraboloid pointing upwards, then $\hat{n}$ covers the same portion of the unit sphere two times, with opposite orientation, giving index zero.

These induce a Berry connection $A_\pm^{\mathbb{S}^2} = -i\langle\psi_\pm|d\psi_\pm\rangle = \mp\cos\theta\, d\phi$ and Berry curvature $F_\pm^{\mathbb{S}^2} = dA_\pm^{\mathbb{S}^2} = \pm\sin\theta\, d\theta \wedge d\phi$. We observe that $F_+^{\mathbb{S}^2}$ is the volume form of the sphere, thus $\mathcal{C}_+ = 1/(2\pi)\int_{\mathbb{R}^2}\hat{n}^* F_+^{\mathbb{S}^2}$ is twice the index (or degree) of the map $\hat{n}$. The index of a map is an integer that counts the signed number of times that the domain (here the momentum space, compactified to a sphere) wraps on the target space (here the sphere $\mathbb{S}^2$). The index of $\hat{n}$ depends on the relative values of K_1^o and K_2^o as follows. When K_1^o and K_2^o have the same sign, the map $\hat{n}$ does not fully cover the sphere, thereby yielding a vanishing index and $\mathcal{C}_+ = 0$. When K_1^o and K_2^o have opposite sign, the map $\hat{n}$ covers the sphere once, so $|\mathcal{C}_+| = 2$. The sign of the Chern number then depends on the orientation of the covering: if $K_2^o > 0$, $\hat{n}(\mathbf{0}) = (0,0,1)^{\mathrm{t}}$, so the sphere is covered from the top and thus $\mathcal{C}_+ = 2$; if $K_2^o < 0$, the sphere is covered from the bottom, leading to $\mathcal{C}_- = -2$. The result is summarized in Eq. (32). A pictorial representation is given in Fig. 8.

APPENDIX F: NUMERICAL DEMONSTRATION OF TOPOLOGICAL EDGE STATE

To validate the existence and properties of the topological edge mode, we numerically solve Eqs. (21) and (22) in the presence of a boundary. For stability, we consider the overdamped limit ($\rho = 0$), and we use the following dimensionless variables: $\tilde{x}_\alpha = \sqrt{12}x_\alpha/h$, $\tilde{w} = \sqrt{12}w/h$, and $\tilde{t} = 12Mt/h^2\Gamma$ where M is an arbitrary reference modulus with dimensions mass/(time^2 × length). With this normalization, Eqs. (21) and (22) read

$$\frac{\partial\tilde{\omega}}{\partial\tilde{t}} = \tilde{\mu}_2\tilde{\nabla}^2\tilde{w} + \tilde{\mu}_2\tilde{\partial}_\alpha\phi_\alpha + \tilde{K}_2^o\epsilon_{\alpha\beta}\tilde{\partial}_\alpha\phi_\beta, \tag{F1}$$

$$\frac{\partial\phi_\alpha}{\partial\tilde{t}} = \left(\tilde{B}\tilde{\partial}_\alpha\tilde{\partial}_\beta + \tilde{\mu}_1\tilde{\nabla}^2\delta_{\alpha\beta} + \tilde{K}_1^o\tilde{\nabla}^2\epsilon_{\alpha\beta}\right)\phi_\beta - \left(\tilde{\mu}_2\delta_{\alpha\beta} + \tilde{K}_2^o\epsilon_{\alpha\beta}\right)(\tilde{\partial}_\beta\tilde{w} + \phi_\beta) + f_\alpha(\tilde{\mathbf{x}},\tilde{t}), \tag{F2}$$

where the the moduli have bee nondimensionalized by M. To drive the system, we have added to the right-hand side of Eq. (22) a forcing term of the form

$$f_1(\tilde{\mathbf{x}},\tilde{t}) = \exp\left[\frac{(\tilde{x}_1 - 20)^2 + \tilde{x}_2^2}{30}\right]\cos(\tilde{\Omega}\tilde{t}), \quad f_2(\tilde{\mathbf{x}},\tilde{t}) = 0, \tag{F3}$$

where $\tilde{\Omega}$ is the driving frequency. The domain of $\tilde{\mathbf{x}}$ is taken to be a hexagon of side length $\sqrt{3}\times 10$, and we discretize the equations onto a triangular lattice and impose the boundary conditions in Eq. (33). The equations of motion are integrated in Python using `scipy.integrate.solve_ivp`. In Fig. 7 we use $\tilde{B} = 0$, $\tilde{\mu}_1 = 0$, $\tilde{K}_2^o = 2$, $\tilde{\mu}_2 = 0.05$. In Figs. 7(a)–7(c) we use $\tilde{K}_1^o = 1$ and in Figs. 7(d)–7(f) we use $\tilde{K}_1^o = -1$. In both panels we take the driving frequency to lie in the predicted bulk band gap $\tilde{\Omega} = 0.1$. The simulations are integrated over a range $\tilde{t} = [0, 300]$. In Fig. 7 the simulation is rendered at time $\tilde{t} = 45$. See Supplemental Movies 1 and 2 [73] for the entire simulation.

APPENDIX G: MAPPING BETWEEN ODD-ELASTIC PLATES AND ODD-VISCOUS FLUIDS

We assume that the dynamics of the active plate is overdamped, which means that inertial terms in the equations [$\rho\omega^2$ in Eq. (25)] can be neglected over the drag term [$i\Gamma\omega$ in Eq. (25)]. We can compare the resulting equations to those of a fluid with odd viscosity exposed to an external magnetic field [54]. For the fluid with odd viscsoity, the physical fields are the density ρ and the velocity $\mathbf{v}$. The parameters are the average density ρ_0, the speed of sound c, a typical frequency ω_B analogous to the cyclotron frequency, the ordinary viscosity ν, and odd viscosity ν^0. The nondimensional linearized Navier-Stokes equations are ([54], Appendix VII)

$$\begin{aligned}\partial_t\mathbf{v} &= -\mathrm{Ma}^{-2}\boldsymbol{\nabla}(\rho/\rho_0) + \mathrm{Ro}^{-1}\mathbf{v}^* + \mathrm{Re}^{-1}\nabla^2\mathbf{v} \\ &\quad + \mathrm{Re}_{\mathrm{odd}}^{-1}\nabla^2\mathbf{v}^*, \\ \partial_t(\rho/\rho_0) &= -\boldsymbol{\nabla}\cdot\mathbf{v},\end{aligned} \tag{G1}$$

where $\mathbf{v}^* \equiv (v_y, -v_x)$ is the velocity rotated by 90° and the Mach, Rossby, Reynolds, and odd Reynolds dimensionless numbers are respectively defined as

$$\mathrm{Ma} = \frac{U}{c}, \quad \mathrm{Ro} = \frac{U}{L\omega_B}, \quad \mathrm{Re} = \frac{UL}{\nu}, \quad \mathrm{Re}_{\mathrm{odd}} = \frac{UL}{\nu^o}. \tag{G2}$$

The nondimensionalized equations of an odd-elastic plate with $\tilde{B} = \mu_2 = 0$ can be obtained defining a timescale T (so that $\partial_t \to T^{-1}\partial_t$) and read

$$\begin{aligned}\partial_t\boldsymbol{\phi} &= -\bar{K}_2^o\boldsymbol{\nabla}^* w - \bar{K}_2^o\boldsymbol{\phi}^* + \bar{\mu}_1\nabla^2\boldsymbol{\phi} + \bar{K}_1^o\nabla^2\boldsymbol{\phi}^*, \\ \partial_t w &= \bar{K}_2^o\boldsymbol{\nabla}\cdot\boldsymbol{\phi}^*\end{aligned} \tag{G3}$$

with

$$\bar{\mu}_1 = \frac{12\mu_1 T}{h^2\Gamma}, \quad \bar{K}_1^o = \frac{12K_1^o T}{h^2\Gamma}, \quad \bar{K}_2^o = \frac{12K_2^o T}{h^2\Gamma}, \tag{G4}$$

and $\boldsymbol{\nabla}^* \equiv (\partial_y, -\partial_x)$. Then the mapping from the odd-elastic plate to the odd-viscous fluid is obtained through the

identification

$$\phi_\alpha = \epsilon_{\alpha\beta} v_\beta, \qquad w = \rho/\rho_0,$$
$$\mathrm{Ma}^{-2} = \bar{K}_2^o, \qquad \mathrm{Ro}^{-1} = -\bar{K}_2^o,$$
$$\mathrm{Re}^{-1} = \bar{\mu}_1, \qquad \mathrm{Re}_{\mathrm{odd}}^{-1} = \bar{K}_1^o,$$
$$1 = \bar{K}_2^o. \tag{G5}$$

In the mapping, the two scalar fields are identified, and the two vector fields are identified (after a rotation by 90°). K_1^o is related to the odd Reynolds number, as they refer to the same tensor component, respectively, for the elastic tensor and for the viscosity tensor. K_2^o is related to ω_B. In fact, K_2^o makes the vector ϕ rotate, as ω_B makes the velocity rotate. The passive shear modulus μ_1 acts as an ordinary shear viscosity term. Finally, the requirement $1 = \bar{K}_2^o$ fixes the timescale of the plate to $T = h^2\Gamma/(12K_2^o)$.

[1] H. Turlier, B. Audoly, J. Prost, and J.-F. Joanny, Biophys. J. **106**, 114 (2014).
[2] R. Phillips, J. Kondev, and J. Theriot, *Physical Biology of the Cell* (Garland Science, Boca Raton, 2009).
[3] J.-L. Maître, H. Berthoumieux, S. F. G. Krens, G. Salbreux, F. Jülicher, E. Paluch, and C.-P. Heisenberg, Science **338**, 253 (2012).
[4] H. Berthoumieux, J.-L. Maître, C.-P. Heisenberg, E. K. Paluch, F. Jülicher, and G. Salbreux, New J. Phys. **16**, 065005 (2014).
[5] J. A. Jackson, N. Romeo, A. Mietke, K. J. Burns, J. F. Totz, A. C. Martin, J. Dunkel, and J. Imran Alsous, Nat. Phys. **19**, 1927 (2023).
[6] F. Jülicher, S. W. Grill, and G. Salbreux, Rep. Prog. Phys. **81**, 076601 (2018).
[7] R. G. Morris and M. Rao, Phys. Rev. E **100**, 022413 (2019).
[8] D. Khoromskaia and G. Salbreux, eLife **12**, e75878 (2023).
[9] B. Shih, D. Shah, J. Li, T. G. Thuruthel, Y.-L. Park, F. Iida, Z. Bao, R. Kramer-Bottiglio, and M. T. Tolley, Sci. Robot. **5**, eaaz9239 (2020).
[10] M. Amjadi, K.-U. Kyung, I. Park, and M. Sitti, Adv. Funct. Mater. **26**, 1678 (2016).
[11] B. K. Johnson, M. Naris, V. Sundaram, A. Volchko, K. Ly, S. K. Mitchell, E. Acome, N. Kellaris, C. Keplinger, N. Correll *et al.*, Nat. Commun. **14**, 4516 (2023).
[12] J. N. Reddy, *Theory and Analysis of Elastic Plates and Shells* (CRC Press, Boca Raton, 2006).
[13] L. Landau, E. Lifshitz, A. Kosevich, J. Sykes, L. Pitaevskii, and W. Reid, *Theory of Elasticity*, Course of Theoretical Physics (Elsevier Science, 1986).
[14] B. Audoly and Y. Pomeau, *Elasticity and Geometry: From Hair Curls to the Non-linear Response of Shells* (Oxford University Press, Oxford, 2010).
[15] H. S. Seung and D. R. Nelson, Phys. Rev. A **38**, 1005 (1988).
[16] S. S. Datta, S.-H. Kim, J. Paulose, A. Abbaspourrad, D. R. Nelson, and D. A. Weitz, Phys. Rev. Lett. **109**, 134302 (2012).
[17] J. Paulose, G. A. Vliegenthart, G. Gompper, and D. R. Nelson, Proc. Natl. Acad. Sci. USA **109**, 19551 (2012).
[18] H. Turlier and T. Betz, Annu. Rev. Condens. Matter Phys. **10**, 213 (2019).
[19] G. Salbreux and F. Jülicher, Phys. Rev. E **96**, 032404 (2017).
[20] G. Salbreux, F. Jülicher, J. Prost, and A. Callan-Jones, Phys. Rev. Res. **4**, 033158 (2022).
[21] D. Needleman and Z. Dogic, Nat. Rev. Mater. **2**, 17048 (2017).
[22] A. Mietke, F. Jülicher, and I. F. Sbalzarini, Proc. Natl. Acad. Sci. USA **116**, 29 (2019).
[23] P. W. Miller, N. Stoop, and J. Dunkel, Phys. Rev. Lett. **120**, 268001 (2018).
[24] G. Gompper, R. G. Winkler, T. Speck, A. Solon, C. Nardini, F. Peruani, H. Löwen, R. Golestanian, U. B. Kaupp, L. Alvarez *et al.*, J. Phys.: Condens. Matter **32**, 193001 (2020).
[25] C. Scheibner, A. Souslov, D. Banerjee, P. Surówka, W. T. M. Irvine, and V. Vitelli, Nat. Phys. **16**, 475 (2020).
[26] M. Fruchart, C. Scheibner, and V. Vitelli, Annu. Rev. Condens. Matter Phys. **14**, 471 (2023).
[27] W. Van Saarloos, V. Vitelli, and Z. Zeravcic, *Soft Matter Concepts, Phenomena and Applications* (Princeton University Press, Princeton, 2023).
[28] Y. Chen, X. Li, C. Scheibner, V. Vitelli, and G. Huang, Nat. Commun. **12**, 5935 (2021).
[29] M. Brandenbourger, C. Scheibner, J. Veenstra, V. Vitelli, and C. Coulais, arXiv:2108.08837.
[30] E. S. Bililign, F. Balboa Usabiaga, Y. A. Ganan, A. Poncet, V. Soni, S. Magkiriadou, M. J. Shelley, D. Bartolo, and W. T. M. Irvine, Nat. Phys. **18**, 212 (2022).
[31] T. H. Tan, A. Mietke, J. Li, Y. Chen, H. Higinbotham, P. J. Foster, S. Gokhale, J. Dunkel, and N. Fakhri, Nature (London) **607**, 287 (2022).
[32] S. Shankar and L. Mahadevan, bioRxiv (2022).
[33] S. Shankar, A. Souslov, M. J. Bowick, M. C. Marchetti, and V. Vitelli, Nat. Rev. Phys. **4**, 380 (2022).
[34] C. Scheibner, W. T. M. Irvine, and V. Vitelli, Phys. Rev. Lett. **125**, 118001 (2020).
[35] C. L. Kane and T. C. Lubensky, Nat. Phys. **10**, 39 (2014).
[36] K. Bertoldi, V. Vitelli, J. Christensen, and M. van Hecke, Nat. Rev. Mater. **2**, 17066 (2017).
[37] S. D. Huber, Nat. Phys. **12**, 621 (2016).
[38] L. M. Nash, D. Kleckner, A. Read, V. Vitelli, A. M. Turner, and W. T. M. Irvine, Proc. Natl. Acad. Sci. USA **112**, 14495 (2015).
[39] P. Wang, L. Lu, and K. Bertoldi, Phys. Rev. Lett. **115**, 104302 (2015).
[40] R. Süsstrunk and S. D. Huber, Science **349**, 47 (2015).
[41] A. Foehr, O. R. Bilal, S. D. Huber, and C. Daraio, Phys. Rev. Lett. **120**, 205501 (2018).
[42] Y. Zhao, X. Zhou, and G. Huang, J. Mech. Phys. Solids **143**, 104065 (2020).
[43] C. Benzoni, B. Jeevanesan, and S. Moroz, Phys. Rev. B **104**, 024435 (2021).
[44] K. Sun and X. Mao, Phys. Rev. Lett. **124**, 207601 (2020).
[45] A. Saremi and Z. Rocklin, Phys. Rev. X **10**, 011052 (2020).
[46] S. Shankar, P. Bryde, and L. Mahadevan, Proc. Natl. Acad. Sci. USA **119**, e2117241119 (2022).

[47] P. G. Ciarlet, *Mathematical Elasticity: Volume II: Theory of Plates* (Elsevier Science, Paris, 1997).
[48] D. D. Fox, A. Raoult, and J. C. Simo, Arch. Ration. Mech. Anal. **124**, 157 (1993).
[49] L. Pitaevskii and E. Lifshitz, *Physical Kinetics* (Elsevier Science, Oxford, 2012), Vol. 10.
[50] C. A. Truesdell, J. Rese. Natl. Bur. Stand. B **67B**, 85 (1963).
[51] L. Braverman, C. Scheibner, B. Van Saders, and V. Vitelli, Phys. Rev. Lett. **127**, 268001 (2021).
[52] At first glance, the assumptions that $\sigma_{zz} = 0$ and $u_{zz} = 0$ at the same time appear inconsistent. This apparent paradox, already present without odd elasticity, is resolved by performing an asymptotic expansion in the plate thickness. Such an analysis produces, at the same time, constitutive relations consistent with plane-stress condition and a kinematic description consistent with the plane-strain condition [47,48].
[53] P. Delplace, J. B. Marston, and A. Venaille, Science **358**, 1075 (2017).
[54] A. Souslov, K. Dasbiswas, M. Fruchart, S. Vaikuntanathan, and V. Vitelli, Phys. Rev. Lett. **122**, 128001 (2019).
[55] C. Tauber, P. Delplace, and A. Venaille, J. Fluid Mech. **868**, R2 (2019).
[56] C. Tauber, P. Delplace, and A. Venaille, Phys. Rev. Res. **2**, 013147 (2020).
[57] L. A. Hoffmann, L. N. Carenza, J. Eckert, and L. Giomi, Sci. Adv. **8**, eabk2712 (2022).
[58] A. Mietke, V. Jemseena, K. V. Kumar, I. F. Sbalzarini, and F. Jülicher, Phys. Rev. Lett. **123**, 188101 (2019).
[59] G. E. Volovik, Sov. Phys. JETP **67**, 1804 (1988).
[60] H. So, Prog. Theor. Phys. **74**, 585 (1985).
[61] A. Coste and M. Lüscher, Nucl. Phys. B **323**, 631 (1989).
[62] G. Bal, J. Math. Phys. **60**, 081506 (2019).
[63] G. Bal, Commun. Partial Diff. Eq. **47**, 1636 (2022).
[64] J. E. Avron, J. Stat. Phys. **92**, 543 (1998).
[65] M. Z. Hasan and C. L. Kane, Rev. Mod. Phys. **82**, 3045 (2010).
[66] D. Banerjee, V. Vitelli, F. Jülicher, and P. Surówka, Phys. Rev. Lett. **126**, 138001 (2021).
[67] R. Lier, J. Armas, S. Bo, C. Duclut, F. Jülicher, and P. Surówka, Phys. Rev. E **105**, 054607 (2022).
[68] C. Floyd, A. R. Dinner, and S. Vaikuntanathan, arXiv:2210.01159.
[69] S. Ramaswamy, J. Toner, and J. Prost, Phys. Rev. Lett. **84**, 3494 (2000).
[70] N. Gov, Phys. Rev. Lett. **93**, 268104 (2004).
[71] G. Salbreux, G. Charras, and E. Paluch, Trends Cell Biol. **22**, 536 (2012).
[72] T. Lecuit and P.-F. Lenne, Nat. Rev. Mol. Cell Biol. **8**, 633 (2007).
[73] See Supplemental Material at http://link.aps.org/supplemental/10.1103/PhysRevE.109.024608 for the Supplemental Movies. Supplemental Movie no. 1 is a rendering of the vibrational modes for a odd elastic membrane with $K_1^o/K_2^o > 0$. The plots are the same as in Figs. 7(a)–7(c). The membrane is topologically trivial, and it is probed in its bulk band gap, and accordingly the deformations do not propagate. See Appendix F for numerical details. Supplemental Movie no. 2 is a rendering of the vibrational modes for a odd elastic membrane with $K_1^o/K_2^o < 0$. The plots are the same as in Figs. 7(d)–7(f). The membrane is topologically nontrivial, and it is probed in its bulk band gap, and accordingly a unidirectional wave travels along its boundary. See Appendix F for numerical details.
[74] https://zenodo.org/doi/10.5281/zenodo.10602231.